DETERMINATION OF THE CRYSTAL PHASE DEPENDENCE ON THE OPTICAL PROPERTIES OF DIAMOND AND GRAPHITE (HOPG) BETWEEN 30 AND 1600 NM

by

Matthew B. Squires

A thesis submitted to the faculty of

Brigham Young University

in partial fulfillment of the requirements for the degree of

Master of Science

Physics and Astronomy Department

Brigham Young University

December 2000

BRIGHAM YOUNG UNIVERSITY

GRADUATE COMMITTEE APPROVAL

of a thesis submitted by

Matthew B. Squires

This thesis has been read by each member of the following graduate committee and by majority vote has been found to be satisfactory.

Date	David D. Allred, Chair
Date	R. Steven Turley
Date	Robert C. Davis

BRIGHAM YOUNG UNIVERSITY

As chair of the candidate's graduate committee, I have read the thesis of Matthew B. Squires in its final form and have found that (1) its format, citations, and bibliographical style are consistent and acceptable and fulfill university and department style requirements; (2) its illustrative materials including figures, tables, and charts are in place; and (3) the final manuscript is satisfactory to the graduate committee and is ready for submission to the university library.

Date

David D. Allred, Chair

Accepted for the Department

Jean-Francois S. Van Huele
Graduate Coordinator

Accepted for the College

Nolan Mangelson
Associate Dean,
College of Physical and Mathematical Sciences

ABSTRACT

DETERMINATION OF THE CRYSTAL PHASE DEPENDENCE
ON THE OPTICAL PROPERTIES OF DIAMOND AND GRAPHITE (HOPG)
BETWEEN 30 AND 1600 NM

Matthew B. Squires
Department of Physics and Astronomy
Master of Science

Outline of Abstract

Built a chamber that can measure VAR from 1.25deg to 85 Deg

Measured Si and the thickness of its oxide in the EUV

Measured Diamond

Performed Analysis on ASF calculated from OC of Diamond and Graphite taken from other sources

Showed the relative error in the ASF in the EUV Visible and IR

ACKNOWLEDGMENTS

More To Come

Contents

List of Figures

List of Tables

Chapter 1

Background and Introduction

Between 1997 and 2001 the EUV research group at BYU has worked on coating surfaces for two space flight applications. This included optimizing high and low reflectance at specific wavelengths and angles. There were several issues that hampered efforts in both projects.

Difficulty making measurements in the EUV slowed both projects. EUV light is strongly absorbed by air so any measurements must be made in a vacuum. This is difficult because the materials and instruments used to make the measurement must be made from vacuum compatible materials. *In sito* alignment and pump down time are other difficulties when working in the EUV. From lessons learned during the completion of the first contract a variable angle reflectometer (VAR) was designed, built, and succesfully used to complete the second contract. The design and construction of the VAR are discussed in this thesis. Measurements of industrial diamond and graphite (HOPG) made using the VAR will be compared to previous measurements of diamond and graphite.

The other main difficulty in completing the contracts were uncertainty in the optical constants of the materials that were used to make the surfaces at extreme ultraviolet (EUV) and vacuum ultraviolet (VUV) wavelengths. In all cases there was disagreement between the published optical constants and the measured optical constants of the materials. In some cases the uncertainty was due to an unknown amount of water absorbed in the films after they were removed from the deposition chamber. Other films grew oxides when they were exposed to air. In some cases the oxides made little difference to the final design and performance of the mirror. In other cases the oxide was the only reason why the films met design specifications [**?**]. In all cases it was difficult to determine which optical constants were valid for an application, and if the material absorbed water or oxygen how to modify the published optical constants to match the observed optical properties.

At lower energies (visible light) and at higher energies (x ray) there are well defined theories to predict the optical properties of a material. This thesis will not entirely ignore low energy theories (i.e. Drude theory) but will concentrate on the theory of atomic scattering factors. Atomic scattering factors are successful at predicting the optical properties of materials in the x ray portion of the electromagnetic spectrum. The theory does break down around absorption edges and in the EUV and visible. This is expected because the theory makes the assumption that the electrons are independent inside the atom. In the EUV and visible this assumption no longer holds. Literature puts the low energy cut off around 50 eV.

But atomic scattering theory is very useful at predicting the optical constants of compounds in the x ray portion of the spectrum. If atomic scattering theory is used to predict the optical constants of material in the EUV what is the error associated with using it? The error can be determined by calculating the relative error between the atomic scattering factors of diamond and graphite. Because diamond and graphite are only different phases of carbon they should have the same atomic scattering factors. Any difference in their atomic scattering factors will show where atomic scattering theory cannot be reliably used.

This thesis will contain two main points: 1)the design, construction, and measurements of the variable angle reflectometer and 2) analysis of the atomic scattering factors for diamond and graphite. Data for industrial diamond and graphite (HOPG) measured using the variable angle reflectometer will not be used in the analysis because previous data sets were more extensive and reliable given that there was not enough time to adequately extend previous work.

Chapter 2

Experimental Setup

The EUV measurements are made using a variable angle reflectometer (VAR) that was designed and built with the help of Cynthia Mills. The operation of the VAR is automated using programs written in LabVIEW. The VAR is connected to a monochromator and a hollow cathode plasma lamp to create the EUV light for the measurements. Figure **??** shows the relative sizes and positions of the VAR, monochromator, and hollow cathode.

2.1 Hollow Cathode

The light source for all the measurements was a McPherson model 692 vacuum UV hollow cathode light source. It is also called a plasma lamp. Light is created by flowing gas into the cathode that is held around -700 volts DC. A plasma is formed in the hollow cathode and the hot gas radiates spectral lines that are specific to the gas. For operating instructions see appendix **??** and reference [23].

Some sputtering occurs inside the hollow cathode because of the plasma. For lighter gases (hydrogen and helium) this is not a serious issue, but heavier gases (argon and neon) will significantly erode

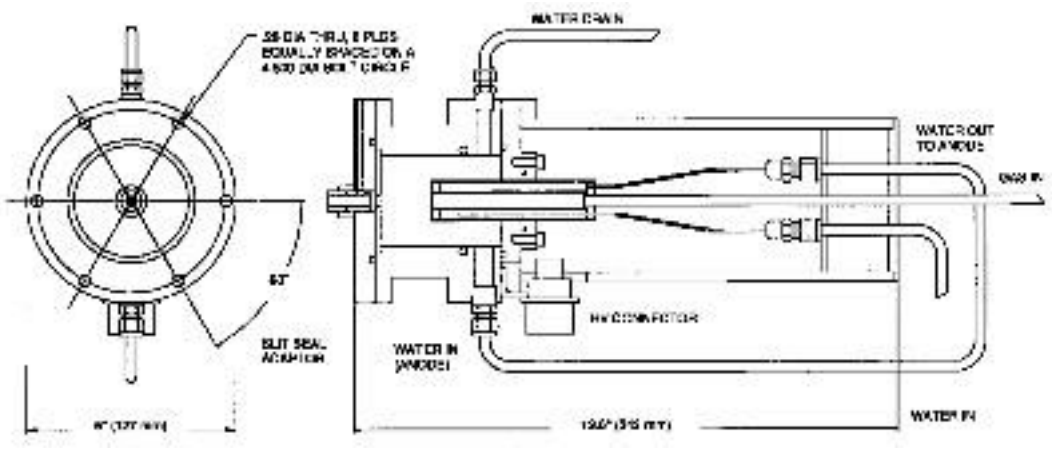

Figure 2.1: Schematic drawing of model 692 VUV hollow cathode light source[24].

the interior walls of the hollow cathode. This has occurred to the point that the cooling water that flows inside the cathode has broken through the walls and flooded the monochromator! This erosion occurs in the tube where the gas flows into the cathode.

2.2 Monochromator

A McPherson model 225 vacuum ultraviolet (VUV) monochromator is used to separate and isolate one wavelength of light from other wavelengths that are also created in the hollow cathode. Its function is similar to a glass prism. White light goes into the prism where the colors separate and come out at different positions. The process by which the light is separated is different but the light seperating principle is the same. There are three essential parts for the operation of the monochromator. The entrance slit, the grating, and the exit slit.

The entrance slit is used to define the beam coming from the plasma lamp. Practically it is used to adjust the amount of light entering the monochromator. The gratings used in the monochromator are concave reflection gratings coated with platnum or magnesium fluoride. In magnesium floride coated grating is used for wavelengths between 450 to 1600 Å, and the platinum coated grating is used for wavelengths between 250 to 1200 Å. The magnesium floride coated grating was exclusively used for all measurements because there was not enough time to clean the platinum grating.

The light that strikes the grating is comprised of several wavelengths of light that depend on the gas that is being used in the hollow cathode. The grating reflects each of these wavelengths at a different angle. By rotating the grating different wavelengths of light will focus on the exit slits. The basic equation for light reflecting off a grating is

$$\sin(\theta) + \sin(\phi) = \frac{n\lambda}{d} \tag{2.1}$$

where λ is the wavelength of interest, d is the distance between grooves on the grating, ϕ is the angle the light strikes the grating, and θ is the angle the light reflects off the surface of the grating. For a rigorous treatment of diffraction see reference [26].

After the light has been diffracted it passes through the exit slits. The position of the slits only allows one wavelength of light to pass though because the exit slit is held at a fixed angle of 7.5^o to the diffraction grating. The width of the exit slit determines the resolution of the monochromator. The wider the slits the more angles (wavelengths) will be able to pass through the slits. The width of the exit slit is typically not a problem because most of the light coming from the hollow cathode is spectral radiation at discrete wavelengths. If a continuous source was used it would be important to keep the exit slit as small as possible. Practically, as with the entrance slits, the exit slit is used to determine the intensity of the light entering the measurement chamber.

2.3 Variable Angle Reflectometer

The variable angle reflectometer (VAR) was primarily built to measure specular reflectance at multiple wavelengths or $\theta\backslash 2\theta$ reflectance scans. It was also designed to be used for future needs, such as non-specular scattering, polarimetry, *in situ* deposition, and surface scans. The chamber is large

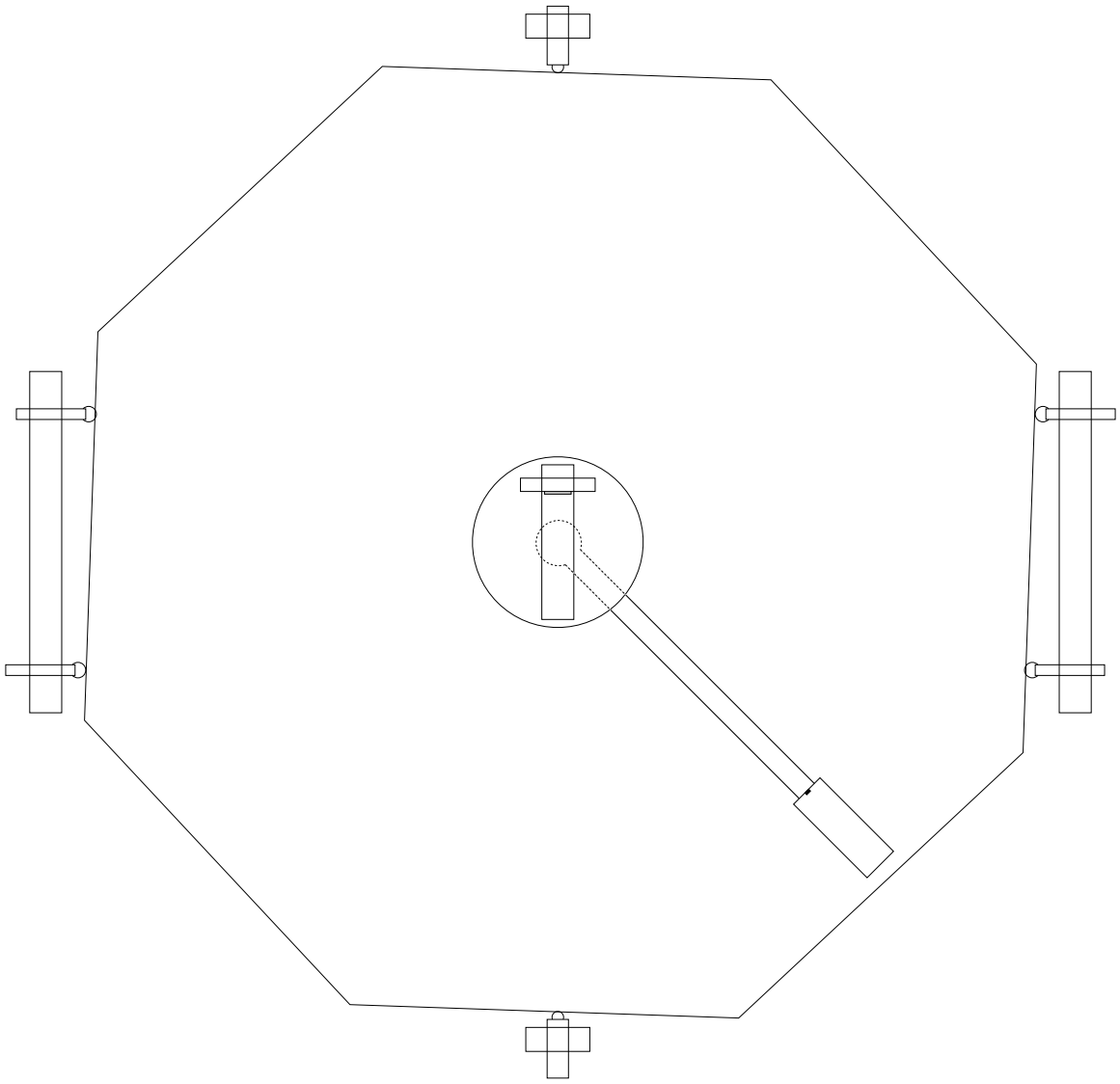

Figure 2.2: Schematic drawing of variable angle reflectometer, including internal and external hardware.

enough to accommodate other equipment and there are enough free ports to add feedthroughs or other external equipment. The VAR was built with several short and long term goals in mind:

- Perform automated $\theta\backslash 2\theta$ scans between 5 and 85 degrees
- Rotate the detector and sample independently
- Move the sample out of the beam to make absolute reflectance measurements
- Scan the surface of the sample to verify uniformity
- Perform *in situ* deposition and measurements
- Interlock to transfer samples into O-chamber
- Polarimetry
- Transmission measurements
- Mount different types of detectors
- Be easily alignable

Not all of these goals have been realized by this writing but all of the goals can be implimented with relative ease.

This section will focus on the design of the VAR and the principles and basics of how the O-chamber is aligned. As mentioned previously the O-chamber was designed to be flexible for future needs. To facilitate future research few parts are permanently fixed to the O-chamber, and as reasonable many elements of the VAR were designed so they could be adjusted to fit future needs.

Making accurate $\theta\backslash 2\theta$ measurements requires accurate alignment of the sample, detector, and light source [Put in the reference from Palik or some other]. The different types of misalignments and their effects are described in the REF TO ERROR ANALYSIS SECTION

The O-chamber is first aligned with the light coming from the monochromator. The sample and detector are then aligned with the O-chamber and monochromator. The full alignment procedure may be found in Appendix **??**.

2.3.1 Vacuum Chamber

The vacuum chamber is connected to the monochromator by a stainless steel bellows that is welded to stainless steel flanges that correspond to the ports on the monochromator and octagonal chamber. The original nipple was a little too short so there was not sufficient room between the octagonal chamber and the hollow cathode. A 1/2 inch spacer place was machined from aluminum that allowed the chamber to be properly aligned with adequate room around the hollow cathode. A mechanical lift was built by Greg Harris to lift the lid off the O-chamber. The chamber should be vented before opening the lid because the lift is strong enough to lift the entire O-chamber. At best it will change the alignment and at worst break the bellows or the hollow cathode.

All parts inside the chamber at mounted on a 1/2 inch aluminum base plate that has holes drilled and tapped on a one inch square grid. This base plate is very convenient because it allows many

different pieces of hardware to be mounted to fixed positions in the O-chamber. The rotation stages, rotational stepper motors, springs, and pinhole are all mounted to the base plate. The base may be positioned inside the chamber by adjusting four lateral pushers. The level or tilt of the base is adjusted by loosening or tightening four set screws mounted in the base plate. The position of the plate may be locked into place inside the chamber by equally tightening all the internal pushers against the walls of the O-chamber.

An electrical feedthrough is used to pass electrical signals to the motors, power the detector, and pass the detector signal out of the chamber. This feedthrough was constrcuted at BYU by Jason Flint and Joseph Young. It was made from a hermetically sealed military feedthrough that surprisingly held a vacuum down to 10^{-4} torr. However this pressure was not acceptable for the operation of the detector. The pins on the vacuum side were extended and a vacuum compatible potting compound was applied to fill any remaining leaks. More details about the feedthrough construction may be found in appendix **??** and reference [27].

The vacuum pressure is measured by a Varian cold cathode gauge that is mounted on the chamber lid and acts as a saftey interlock for the channeltron dector. The chamber is vented though a valve that is also mounted on the lid.

2.3.2 Exterior Alignment Hardware

The chamber is supported on a table that is used to adjust the height, angle, and lateral position of the O-chamber relative to the monochromator. The height and level of the chamber are adjusted by individually changing the height of the table legs. A carpenters level is used to level the table by checking the level of the table along orthogonal directions. If the table is level the floor of the chamber should also be level. That was checked the first time the O-chamber was levelled before the base was installed in the chamber. The level of the chamber is important but the level of the optical base in the VAR is much more important that the level of the table or VAR.

The lateral position of the VAR is adjusted by loosening and tightening screws in opposite lateral alignment blocks (see Figure 4.20). The angular alignment is changed by using the angular alignment blocks. The angle is changed by loosening and tightening the four screws in the angular alignment blocks. Changing the lateral alignment will change the angular alignment and visa versa. A good alignment may take several iterations of lateral and angular alignments.

2.3.3 Alignment of Monochromator and Measurement Chamber

Set up a laser on a isolated table with the VAR chamber is table moved out of the way. The monochromator grating should be moved to zero angstroms so all zero order reflections may come out of the exit slit. Align the laser so it passes through the exit slits, reflects off the center of the grating, and comes out the entrance slits. If the laser does not come out vertically centered the grating may need to be aligned. Consult the McPherson manuals for instructions on aligning the grating. The laser is now the reference for all alignments.

Center the VAR between the lateral and rotational alignment blocks by eye. Move the table and VAR into the beam of the laser so the laser passes through the cross hairs and the retroreflection from the cross hairs roughly returns to the laser. Bolt the bellows onto the monochromator. If the vertical

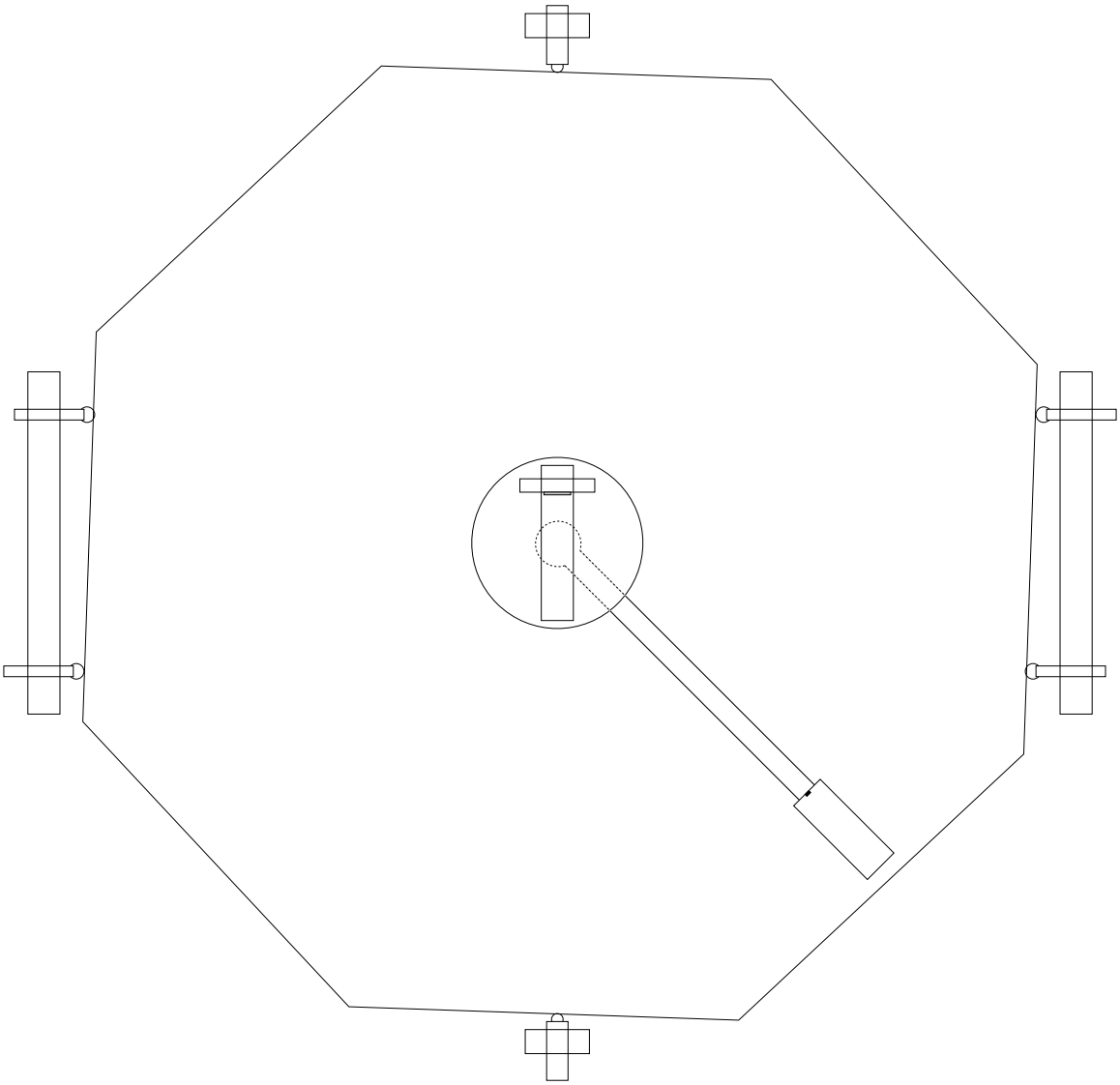

Figure 2.3: Schematic drawing of variable angle reflectometer with external hardware.

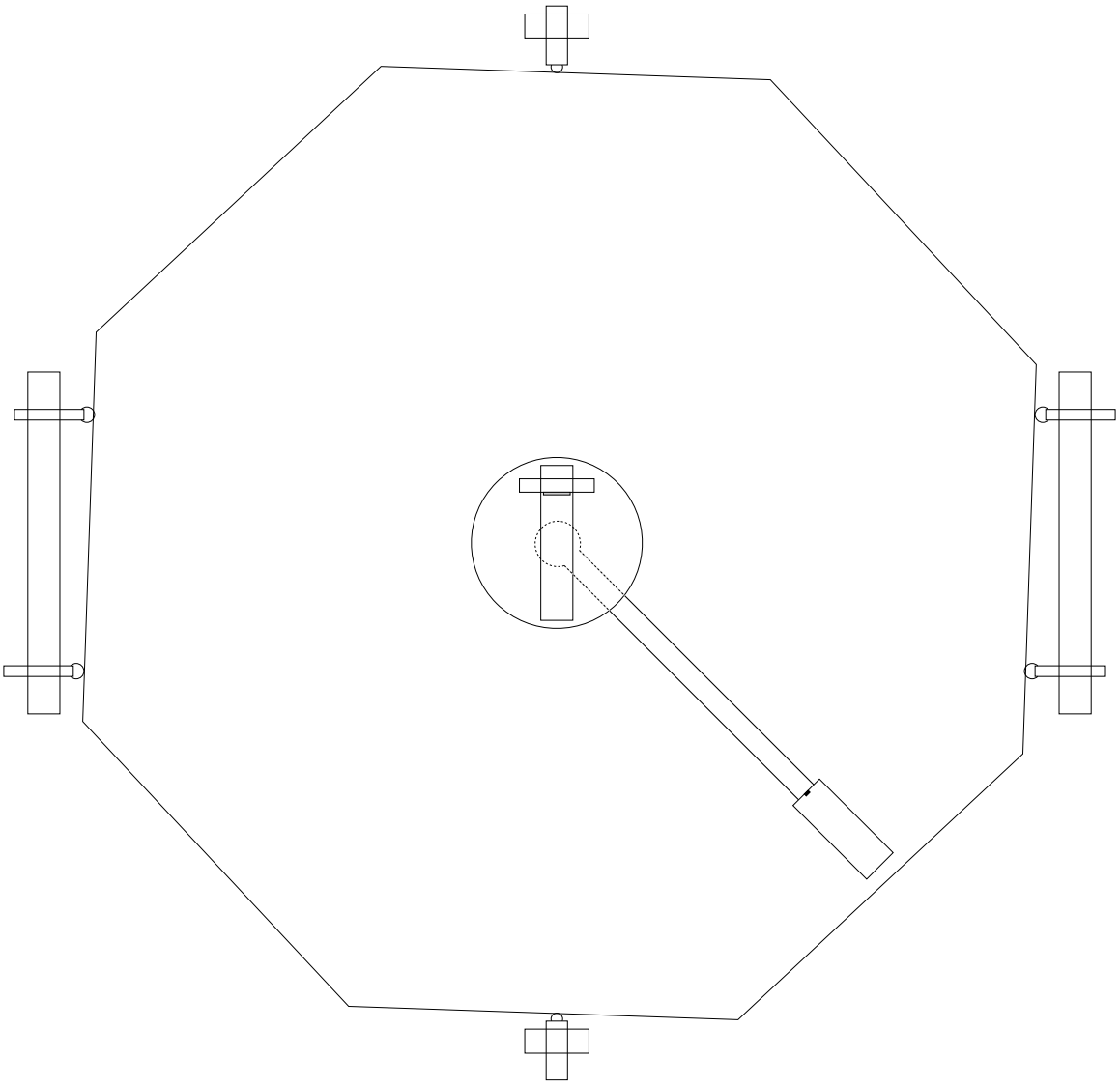

Figure 2.4: Schematic drawing of variable angle reflectometer with external hardware.

alignment is off adjust the height of the table legs till the VAR is aligned in the vertical direction. Using the lateral and rotational alignment blocks align the VAR in the horizontal direction.

It is very important that laser exactly retroreflects off the cross hairs because the cross hairs become the reference for major and minor alignments in the chamber. The laser can now be attached to the VAR table for easier use. A full alignment procedure is found in appendix **??**.

2.3.4 Internal Alignment using Interior Alignment Hardware

As a general practice the interior hardware should be aligned or realigned after the O-chamber has been aligned with the monochromator. The interior hardware can be aligned with the O-chamber independent of the monochromator, but if the table is moved it may change the alignment of the interior hardware. There are two parts to aligning the interior hardware. Levelling the optical base

and aligning the center of rotation with the laser.

The optical base is levelled by adjusting four set screws that are mounted in the optical base in front of the interior alignment blocks. If the base if has not be previously leveled use a carpenters level to roughly level the base. This angle of the base is changed by raising and lowering opposite set screws the base can be levelled in any direction. The monochromator may not be perfectly level, so using a level is only the first step in aligning the VAR.

A laser is used to fine tune the level of the base. The laser is aligned perpendicular to the cross hairs on the back of the chamber. This defines what will be the path of light coming from the monochromator. Put a mirror in the sample stage. If the laser able to reflect off the mirror and return along the same path the optical base is aligned with the laser and the cross hairs. If the laser does not return along the same path the optical base may be aligned by adjusting the set screws.

After the base has been leveled check to make sure the mirror is properly aligned with the detector. Swing the detector around till the laser is shining directly into the opening (This may require removing the rotational motors.) Move the mirror into the beam and rotate the mirror and detector so the laser shines into the detector. The laser should hit the same spot on the detector both times. If it doesn't the mirror angle can be adjusted by loosening and tightening the screws on the base of the z translation stage. Similar to other alignments this alignment may need to be refined using light from the monochromator.

Next align the center of rotation with a plumb bob. The laser is aligned with cross hairs and a plum bob is hung inside the chamber with the laser centered on the string. The optical base can be moved laterally using the interior alignment blocks till the center of rotation is directly beneath the plum bob. The mirror can also be used to align the center of rotation. Adjust the mirror so the laser is just grazing the surface of the mirror. Rotate the mirror 180^o (The length of the cables that are connected to the XYZ stage may need to be lengthened). The laser should also just graze the surface of the mirror after it was rotated.

The position of the optical base is "locked" into place by tightening all of the interior alignment blocks into the walls of the O-chamber. Some care needs to be taken to preserve the alignment when locking the optical base into place. It is important to have the internal alignment blocks push directly into the walls without rotating. Any rotation in the blocks while pushing against the wall will change the level of the optical base. The original interior alignment blocks were screws with brass buttons on the ends to try to eliminate rotation due to friction. The brass buttons did not prevent the base from rotating and were redesigned. Even though the current blocks are slightly more complicated it is necessary for the interior alignment blocks to push on the wall without rotating.

2.3.5 Shaping the Beam with a Pin Hole

The beam coming from the monochromator is divergent with a cone angle of $\sim 3^o$. This causes several problems: 1) the beam will reflect off the mirror and into the detector even when the mirror is moved 15 mm out of the beam, 2) the beam will overfill small samples limiting the size of samples that may be used, 3) this also limits the smallest angle that may be used for analysis, and 4) there is more scattered light in the chamber. To solve these problems a pin hole is placed in the path of the light to narrow the beam. Using a pinhole also has the benefit of being a second reference point

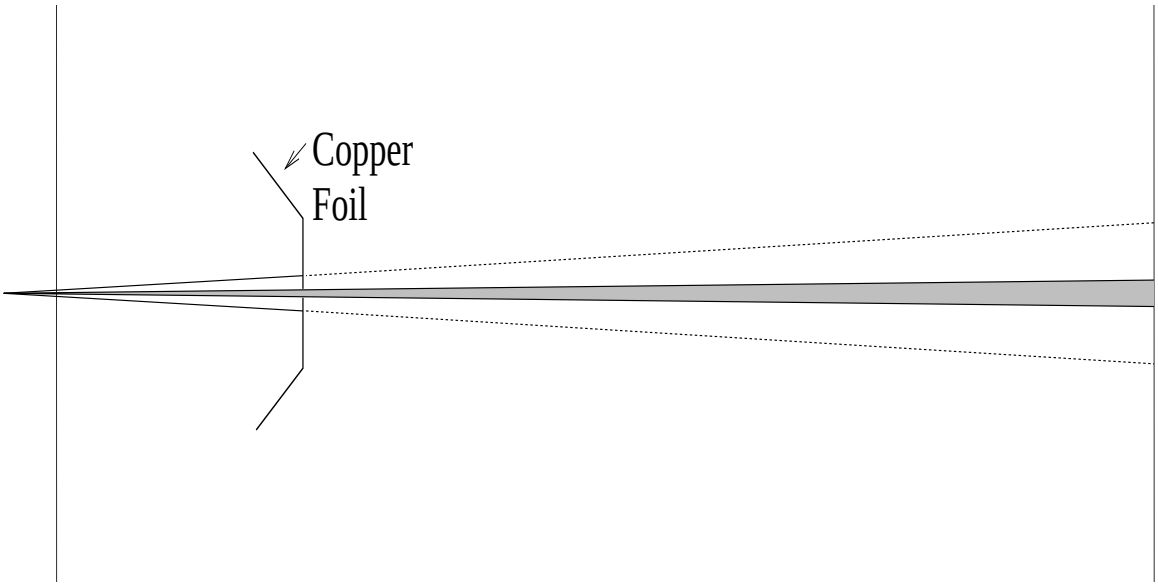

Figure 2.5: Schematic of pinhole redefining the beam from the monochromator.

for the laser in the O-chamber. Because the size of the hole is much larger than EUV wavelengths it is assumed diffraction is a small effect and is ignored.

The pinhole is aligned using a small translation stage mounted to the baseplate. The laser is centered on the pin hole by monitoring the intensity of the laser coming through the pinhole. The vertical and lateral position can be adjusted till the intensity is maximized. The position of the pinhole will determine what part of the beam is sampled[1]. If the pinhole is not aligned there will be a shoulder on one side of the source beam profile. This can slightly be seen on the left side of the most intense beam in figure 2.3.5.

If may be asked if the pinhole will change the width of the beam if the widths of the entrance and exit slits are changed. If the width of the beam profile changes at full width half max (FWHM) or at full width full max (FWFM) then the pin hole is changing the beam profile in a non-reproducable way. Figure 2.3.5 shows two sets of data that are normallised to unity by dividing by the intensity at the peak of each curve. Despite different slit sizes and source intensities (see figure 2.3.5) the two curves are identical. Figure 2.3.5 also shows the signal to off peak noise ratio is about 1 part in 10^3. It can also be seen that the curve that corresponds to the lower intensity is slightly more noisy off as would be expected if the beam was ruled by Gaussian or Poissionian statistics.

With a pinhole of about 1 mm it can also be seen that at FWHM to beam is about 1.5^o and at the detector the beam is about mm wide. The the crosshairs on the back of the chamber it should be about mm wide. The width of the beam at FWFM is about 1.5^o, SO MANY mm at the detector, and SO MANY mm at the crosshairs.

[1]The position of the pinhole may be used to aim the path of the light in the chamber. I know this should work but I have not explored what errors, if any, it introduces.

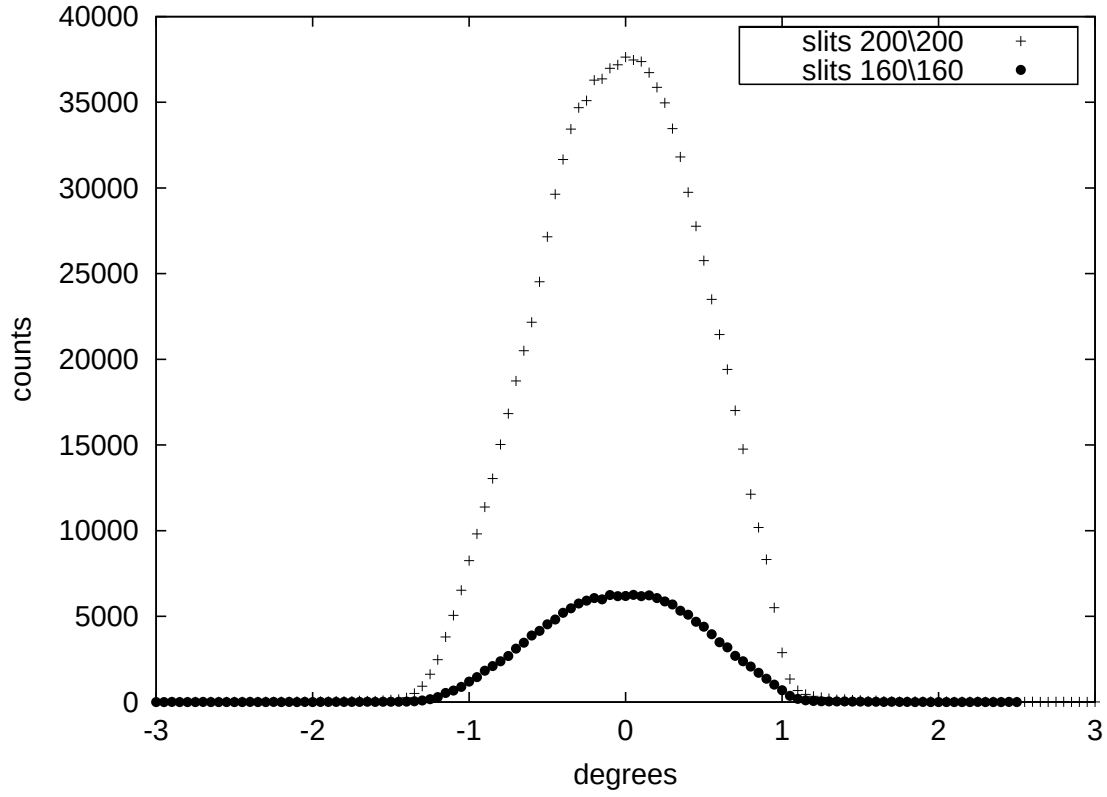

Figure 2.6: Measured angular width of beam after pinhole. The slits widths are reported as (entrance\exit) in μm. The size of the pinhole used for all measurements is SO MANY mm.

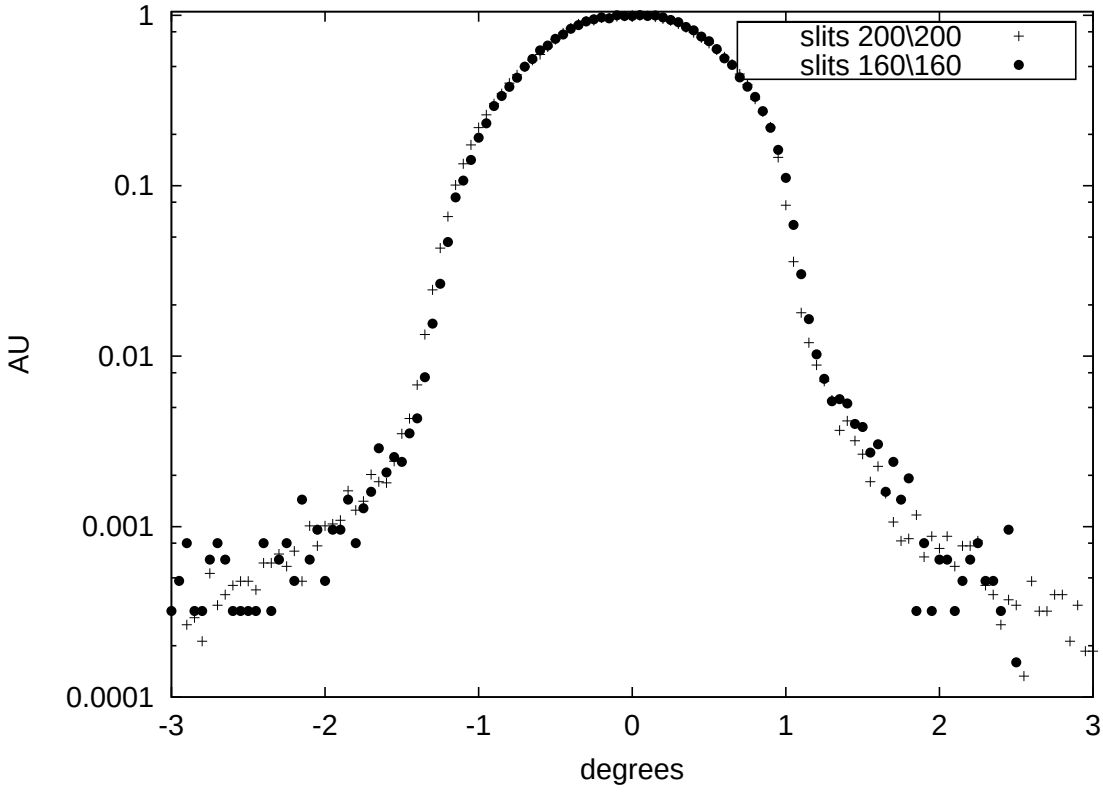

Figure 2.7: Measured angular width of beam after pinhole. The slits widths are reported as (entrance\exit) in μm. The size of the pinhole used for all measurements is SO MANY mm.

2.3.6 Rotation Stages

To get the $\theta\backslash 2\theta$ sample detector movement and independent sample detector movement there needed to two distinct rotation stages that could be moved independent of all other parts. Cynthia Mills looked for commercial rotation stages, but could not find rotation stages that would be able to rotate 180 degrees with no coarse adjustments and would meet the space constraints of the chamber. Because there were no commercial parts available Cynthia and Wes Lifferth designed and the Wes machined the two rotational parts. The mechanical drawing for the rotation stages may be found in appendix **??**.

2.3.7 Translation Stages

An XYZ translation stage was built to make it possible to move the sample out of the beam path, and if desired scan the beam across the sample to check for uniformity. The stage was built by Cynthia Mills using a design that Dr. Peatross had previously used. He gave us a part that attaches the Z stage to the X and Y stages. The stages are moved by stepper motors purchased from Haydon Switch and Instrument. The carriages were made by Techno-Isel Linear Motion Components. The carriages use ball bearings to reduce the friction while keeping the carriage fairly stable. These ball bearing can pop out when the carriage is being placed on the rail. Work over a cloth or towel so if a bearing does escape it is not lost. The bearings can be pushed back into their original position very easily.

2.3.8 Channeltron Detector

A model MD-501 Amptecktron made by Amptek Inc. is used to measure the intensity of the light. The MD-501 uses a channel electron multiplier (CEM) to detect light. The CEM works by creating an electron avalanche of 10^7 electrons for every one photon. The avalanche is initiated when a photon strikes the opening of the CEM. If the photon has enough energy it will eject one or more electrons from the surface of the CEM. That electron is accelerated by a high voltage to the other side of the CEM where it ejects more electrons that cascade inside the CEM till they exit and are detected (see figure 2.8.

The CEM is integrated in a package that contains all the necessary electronics to supply the high voltage that drive the CEM and then amplify and shape the output signal. The MD-501 has a dark count of less than one count/sec. This dark count is ignored in all measurements because it is so small.

It is important to be very careful when operating the MD-501 because the CEM requires 2.4kV to operate[2]. The MD-501 *must* be operated at a pressure lower than 1×10^{-4}torr or the high voltage will create a plasma in the CEM that will act like a short circuit and destroy the electronics in the MD-501. The plasma is a bad for the CEM because it can erode the walls of the CEM.

[2]It is always a good idea to be careful around high voltages, but from my experience the MD-501 is not lethal under normal circumstances. It does HURT like the dickens if you happen to touch it.

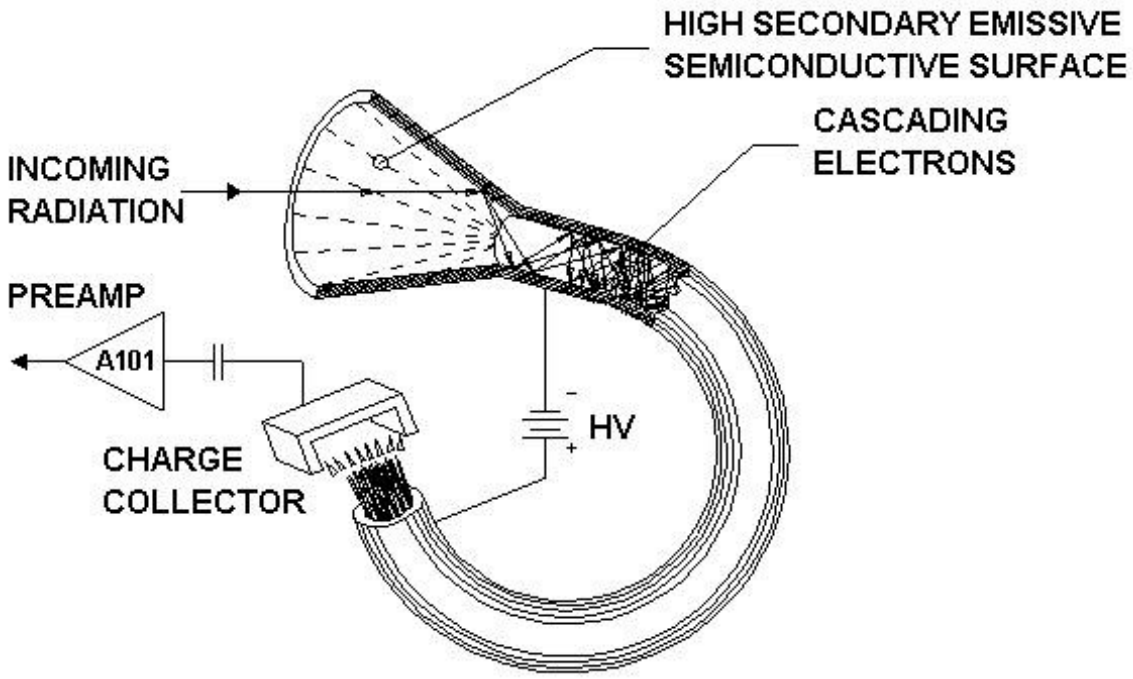

Figure 2.8: Schematic of CEM operation [1].

2.4 LabVIEW Programs

Making measurements by hand is a difficult and error prone process. By automating the process it is faster to make measurements and easier to account for source fluctuations in the calculation of the reflectance. This was done using the LabVIEW software and a National Instrument Data Acquisition board (NIDAQ). Several programs were used to make the measurements. This section will only outline how the key components of the programs work. There are three main programs: FindMax, T2T (Theta 2 Theta), and VAR (Variable Angle Reflectance). In the future these file names may change but the concept of making measurements should be the same.

The LabVIEW virtual instrument (VI) that was used to make all the measurements was built on around FindMax.VI to find the peak of the reflected beam. Because of round off in the subVI that controls the motors it was necessary to make sure the detector was centered on the beam each time it made a measurement. Most of the time spend in making the measurements is finding the maximum position of the beam. Figure 2.4 outlines the process the process for finding the maximum intensity of the beam.

The FindMax.VI is used in T2T.VI a $\theta\backslash 2\theta$ program that will perform a simple theta two theta reflectance scan. This subVI is not a workhorse like FindMax.VI, but simplifies programming a more complex reflectance scan that checks the source intensity at various times during a multiple angle reflectance measurement. Figure 2.4 shows the process of making a $\theta\backslash 2\theta$ scan.

The VAR VI combines all these programs and is entirely automated after the mirror and detector are initially aligned. It checks the source intensity several times during the measurement and records the time when the measurements were made to take into consideration the time varying fluctuations

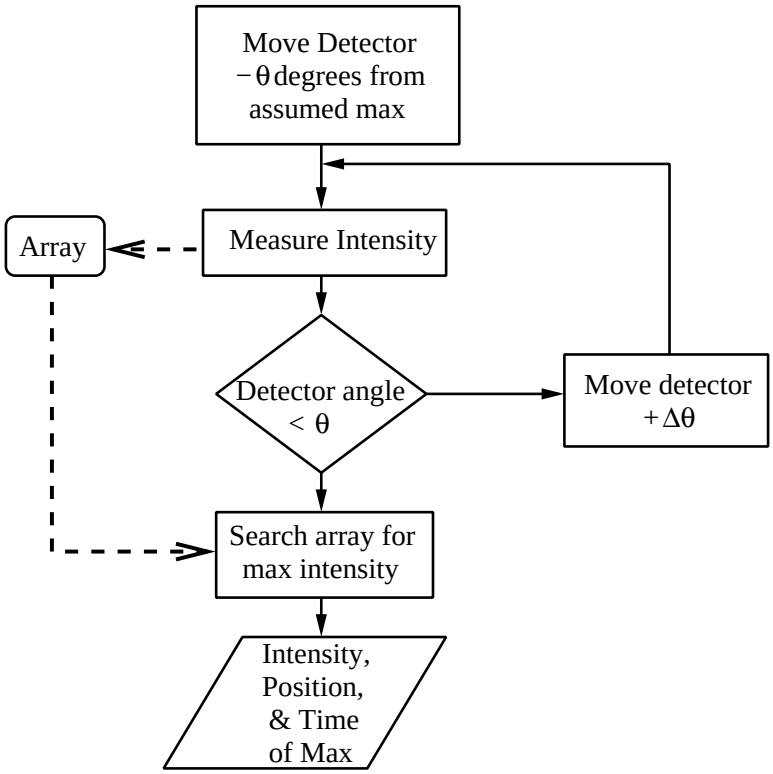

Figure 2.9: Flowchart of FindMax subVI.

of the source. It also calls others subVI's to perform data analysis and make graphics files. The data analysis is explained in section 4.20. Figure 2.4 shows the process VAR.VI follows to take data.

All the LabVIEW programs may be found in appendix **??**. They are also backed up on the CD that should come with this thesis and at XUV.BYU.EDU\thesis.

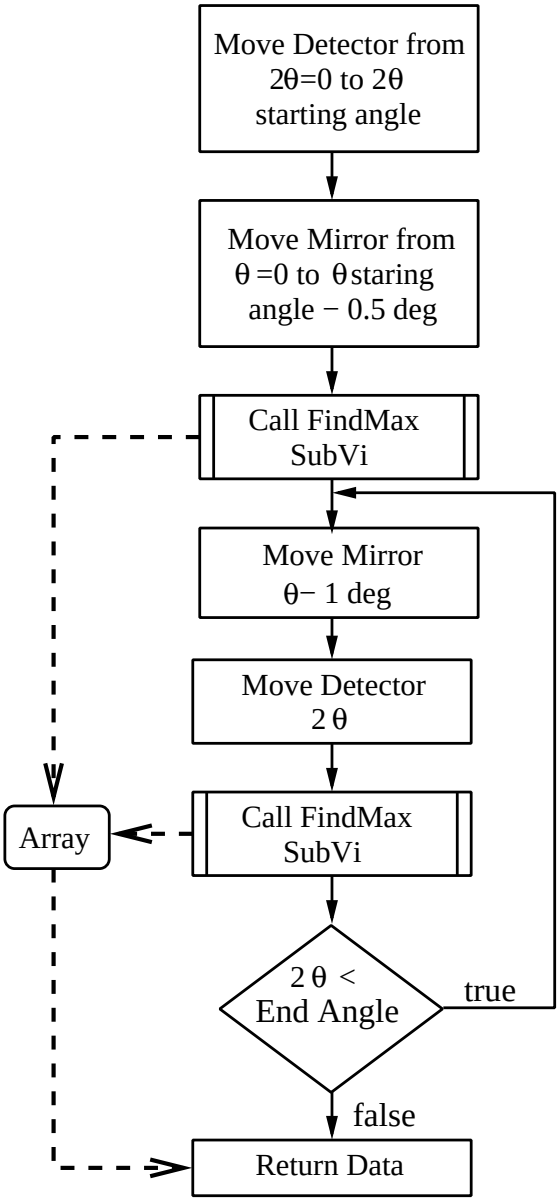

Figure 2.10: Flowchart of T2T subVI.

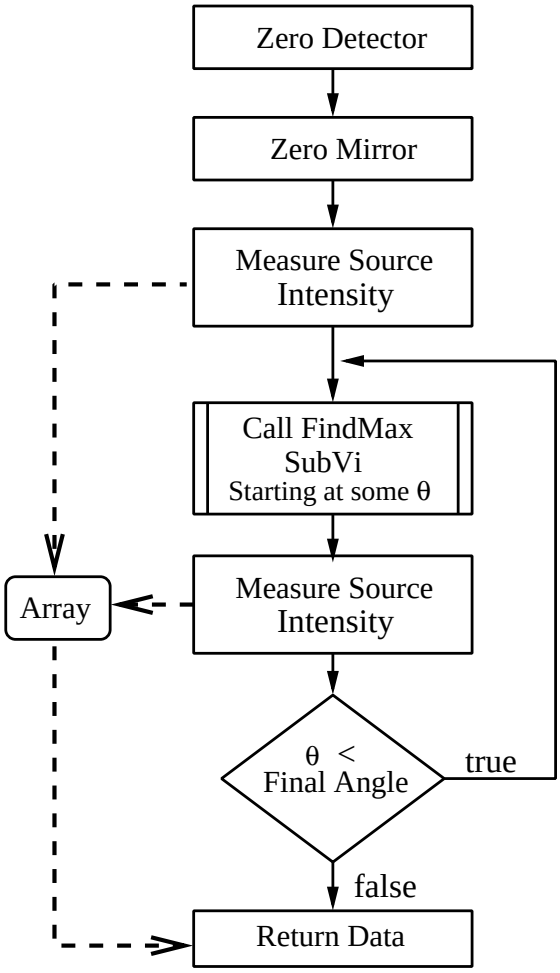

Figure 2.11: Flowchart of VAR subVI.

Chapter 3

Data Analysis on Measurements Made Using VAR

This chapter will show a summary of the optical constants determined from the data taken using the VAR and will largely focus on the analysis used to calculate the optical constants from the measurements. Plots of the reflectance data and the confidence intervals are found in Appendix 4.20. Figure 3 shows a typical reflectance measurement that has been used to fit the optical constants of the material. This data has been adjusted for irregularities in the surface of the diamond as will be explained in Section 3.2.2.

3.1 Summary of Measured Data

	diamond				HOPG			
$\lambda(\AA)$	n	Δ n	k	Δ k	n	Δ n	k	Δ k
584	0.87	0.30	1.23	0.06	1.34	0.25	1.02	0.12
1025	1.38	err	1.22	err	1.42	0.15	0.63	0.11
1084	1.92	0.05	1.45	0.005	1.12	err	0.42	err
1134	1.98	0.07	1.32	0.02	1.63	0.05	0.17	0.12
1164	1.51	0.25	1.03	0.10	1.59	0.07	0.05	0.14
1199	2.08	0.06	0.99	0.02	1.43	0.07	0.20	0.14
1216	1.77	0.12	1.12	0.005	1.45	0.13	0.48	0.11
1640	2.05	0.29	1.07	0.10	0.97	0.17	0.40	0.10

3.2 Fitting Considerations

Fitting data to a complicated model is at best an art. Some of the "art" required may be avoided by making the model to be fit as simple as possible. This thesis was designed to use single bulk layers of a material to make the fitting model as simple as possible. This geometry is best suited for measuring the real part of the index of refraction, the imaginary part may also be determined

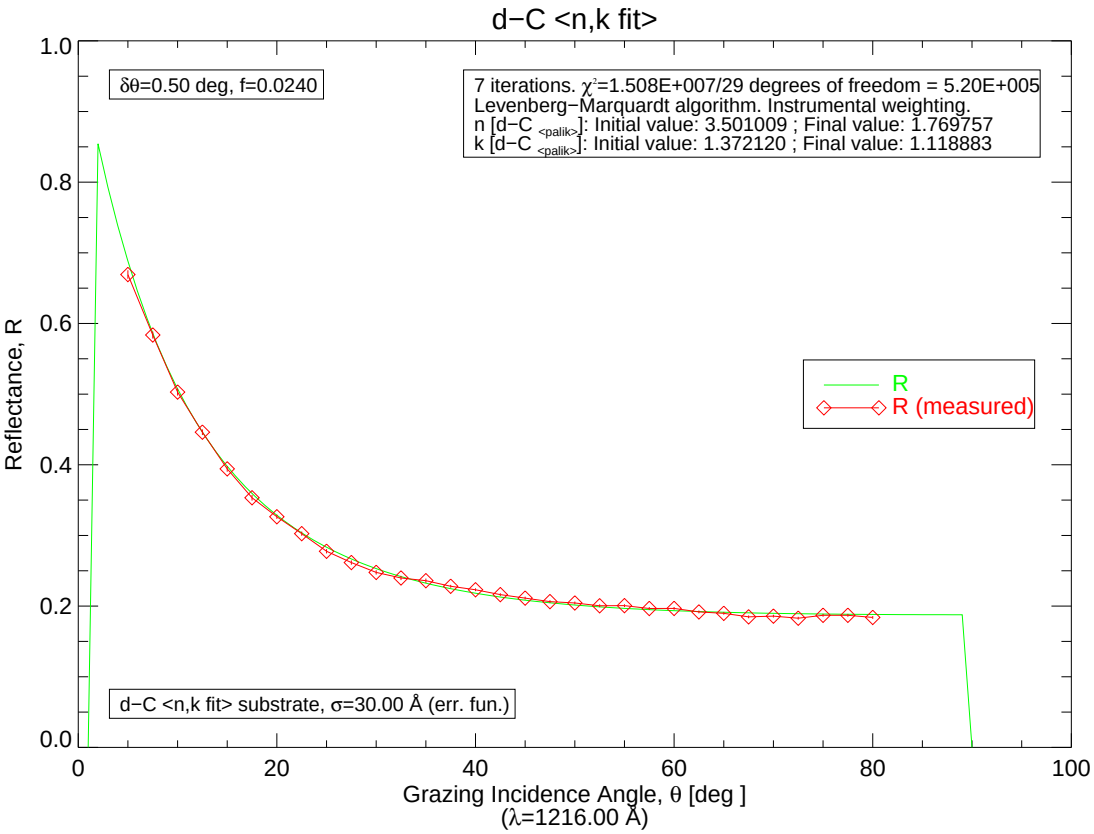

Figure 3.1: Variable angle reflectance data for diamond at 1216 Å.

Original		Fit		Original		Fit	
n	k	n	k	n	k	n	k
0.601	0.010	0.601000	0.009999	1.111	0.010	1.111000	0.010000
	0.111		0.111000		0.111		0.111000
	0.333		0.333000		0.333		0.333000
	1.111		1.111000		1.111		1.111000
	2.222		2.222000		2.222		2.222000
1.333	0.010	1.333000	0.010000	1.699	0.010	1.699000	0.010000
	0.111		0.111000		0.111		0.111000
	0.333		0.333000		0.333		0.333000
	1.111		1.111000		1.111		1.111000
	2.222		2.222000		2.222		2.222000

Table 3.1: Computational results of fitting dummy indices of refraction to contrived data, using the initial values $n, k = 1$.

by transmission through a film of known thickness. Reflecting off a bulk sample will only give the optical constants for the bulk material. The optical constants of a thin film may differ from those of the bulk material, but the object of this thesis is to determine the phase dependence of optical constants. For more on the optical constants of thin films see reference [10].

3.2.1 Uniqueness of Solution

It is important to address the question of uniqueness, because a fit of the data may look good to the eye or even have a low χ^2, but there may be several combinations of n and k that will fit the data well. This is known as finding a local minimum (or maximum depending of the application) instead of a global minimum. This problem has been addressed before and there are many known ways to find global extrema [28]. But it is very difficult to verify if the "best" fit is truly the value that nature would also use.

A simple way to see if there is one good solution to a set of data is to calculate a set of data using a well defined set of optical constants. Then put the calculated data back into IMD, but with the wrong initial conditions and then fit the contrived data to see if it fits the same data to the original n and k. If the fit values of n and k match or are close to the original, even if initial conditions are obviously wrong, it may be assumed the n and k determined from the fit are unique. This is by no means a proof that the fit values are unique but it is a simple test to show how much a fit number may be trusted to be unique. The following table shows that in all cases except for when $n = 0.601$ and $k = 0.010$ the fit optical constants matches the original optical constants accurate to three(?) decimal places. The initial n and k used for the fits are 1 and 1[1]. These are both very generic values for n and k and the results of the table show that these initial conditions will fit any range of n and k to be found in the EUV. This is only shown for a single bulk material. Fitting the optical constants and thicknesses of various thin layers will not always yield a unique result.

The results of table 3.2.1 are based on contrived data that was calculated using IMD. In real life the data will not be smooth, but may have regions where there is significant error in the data. Ignoring

[1]Originally the initial value of k was zero, but IMD warned a small original value is a bad starting point. I tried it anyway, and it was a bad place to start, so I chose k to be the next positive integer, one.

	Original	Fit	Error
n	0.601	0.594096	1.1%
k	0.010	0.010996	9.9%

Table 3.2: Compare good reflectance data with erratic reflectance data.

the error bars that may be calculated, will the values of fit optical constants still be reasonable? To provide one possible answer to the question take one set of calculated data from table 3.2.1 and manually add some scatter to the data. Then, as before, fit the data using the initial optical constants $n, k = 1$. The fit does not match the original optical constants, but the data is flawed at several places. Data that is as obviously flawed as the data in figure **??** should be remeasured. The error in n is acceptable, but there is quite a large error in k. The value of χ^2 is larger than the χ^2 of a smooth set of data.

3.2.2 Fitting Model

Surface Roughness

The surface roughness is one parameter of the fitting model that was measured using atomic force microscopy (AFM) (reference ?). Because the surface roughness has been measured using an external method it does not have to be fit to the model. This reduces the number of fitting parameters, and AFM is the preferd method for quantifying the surface roughness.

It is also important to know the surface roughness because it can make k appear to be larger than what it really is. If light is scattered into another direction by an irregularity on the surface it will not go into the detector, just the same as if it had been absorbed into the material. The surface roughness will also affect the determination of n because the surface will appear to be less reflective, giving the surface an effectively lower n. The relative changes in the surface roughness have to be on the order of tens of angstroms before the effect on the optical constants is large enough to be obviously wrong. But to accurately determine the optical constants it is important to include roughness in the model that will be used to determine the optical constants

The surface roughness is calculated from the calculated power spectral density (PSD). The PSD is calculated by taking the Fourier transform (FT) of the features on the surface of the sample. Because there is roughness over different length scales there is periodic fluctuations on the surface of the sample. The FT by differentiating the frequency content of the surface is able to determine the roughness over a large and small scales (see Reference ?). The roughness is calculated from the PSD by

$$somethinghere \tag{3.1}$$

Diamond (Industrial Fused)

Industrial diamond made from fused diamond micro-crystals was used for all the measurements in this thesis. After the diamond was fused together it is assumed the surface of the diamond was polished using a diamond paste. Because of the polishing a significant amount of roughness was expected. What was unexpected were deep pits that cover the surface of the sample (see Figure

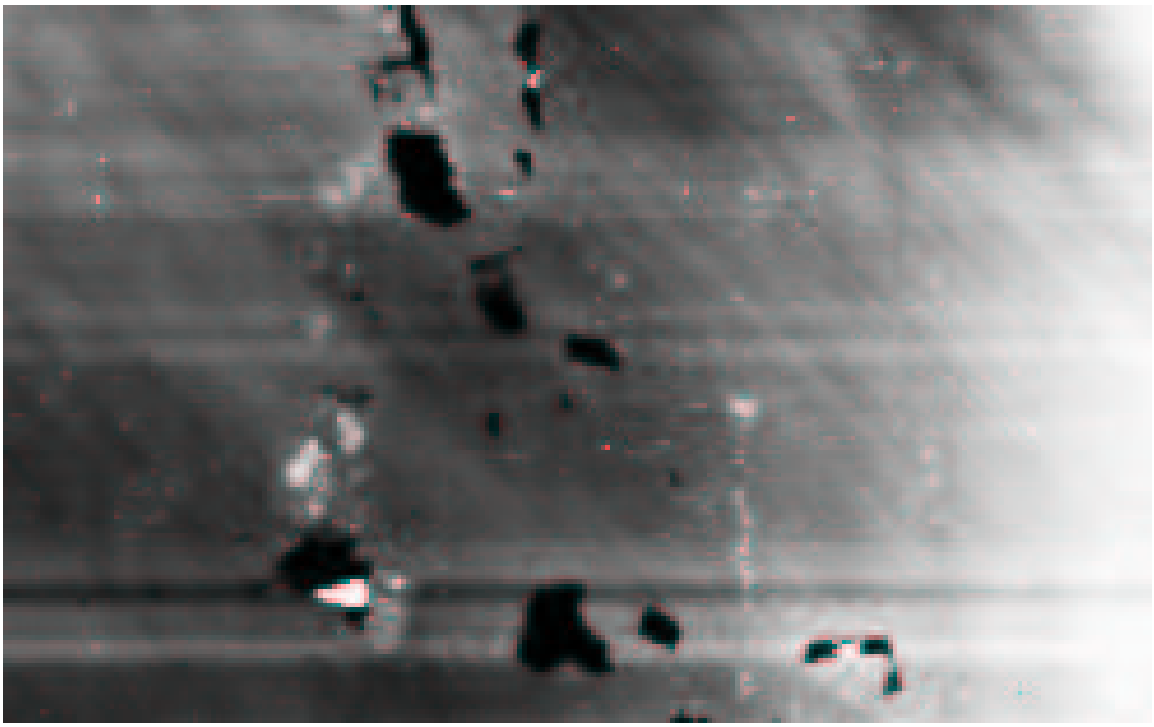

Figure 3.2: AFM image of diamond showing the pits on the surface. The pits take up approximately 2% of the surface. The lines that cross the image diagonally are assumed to be from the polishing.

3.2). The pits do not completely obscure the surface because the areas between the pits are flat from the polishing. The sides of the pits are sufficiently steep and the bottoms are rough so it is assumed that any light that enters a pit will be scattered into all directions. The effect of these pits is to reduce the area of the diamond that will reflect light. This effective area changes with angle because the apparent size of the pits will go like $\sin\theta$.

The area of the sample that is covered with pits is calculated by importing the AFM image into MATLAB and counting the number of pixels that are black by calculating a histogram of the intensity of the pixels (see Figure 3.3) This was done using a simple program that can be found in Appendix 4.20. The pits cover about 2% of the surface of this image. This image is representative of the whole surface of the diamond.

All the diamond data was modified by the following function. The extra term is put in the denominator because the measured reflectance will be small than it should be if there are pits on the surface of the sample.

$$R_m = \frac{R}{(1 - 0.02\sin\theta)} \tag{3.2}$$

The surface roughness of the flat areas between the pits was determined by PSD to be about 30 Å rms roughness.

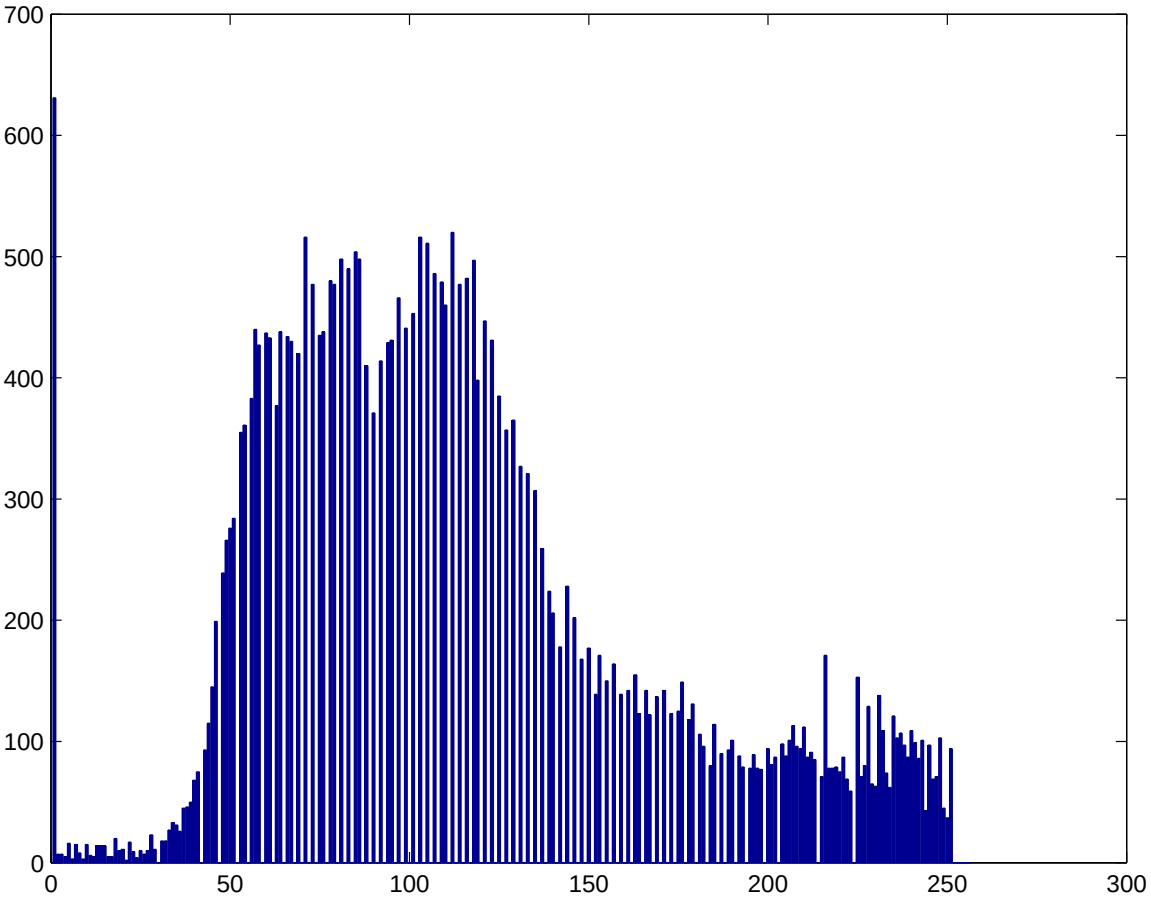

Figure 3.3: Histogram of AFM image to determine what fraction of the surface is covered by pits. The number of black pixels in the first bin is about 630 and the size of the image is 135 x 248, so about 2% of the surface is covered by pits.

Graphite (HOPG)

The surface roughness of the graphite was small enough that the background noise was the significant contribution to the noise. The resolution of the AFM is at worst one or twoÅ, so it is assumed the roughness of the graphite is zero.

3.3 Error Analysis

To accurately describe the optical properties of a material it is necessary to report the measured value and the error associated with the determination of the reported value. This thesis is not meant to explain the statistical details, but it is important to explain the statistical methods used in fitting the optical constants. It is also important for anyone who wants to understand the statistics that is used in the LabVIEW VI's. The standard error, SE, will be used as an approximation to σ the standard deviation in fitting the optical constants and calculating the confidence intervals. IMD will be used to fit the optical constants and calculate confidence intervals based on the χ^2 test to verify the reported error bars.

Two sources of error will be considered in calculating SE. Any other error due to misalignment of the apparatus is assumed to be negligible (see chapter ??? for alignment details.) The first error is due to the counting of individual photons entering the detector during a beam intensity measurement. This type of error is often known as "shot noise" and is described by a Poisson distribution. For large numbers of counts ($n > 1000$) a Poisson distribution approaches a Gaussian distribution [29]. Assuming that there are enough counts and that Gaussian statistics are sufficient, the error contribution due to "shot noise" is given by

$$\sigma = \sqrt{(n)} \tag{3.3}$$

3.3.1 Time Dependent Source Variations

The second source of error is caused by the time variations of the source intensity. For unknown reasons, the intensity of the source may be constant, increase, or decrease over time. In other measurement systems this is reconciled by using a second detector to measure the intensity of the beam before it reflects off the sample. This second detector is used to normalize the source intensity at the same time the reflected intensity is measured. In general this would be the preferred method for monitoring the fluctuations of the source intensity. Due to time and other constraints a second detector was never installed. To account for the time variations of the source, the source intensity is measured at different times during the measurement of a sample and then the source intensity is fit to a line.

The General Polynomial Fit VI from the Mathematics, Fitting section of LabVIEW is used to fit the source intensity measurements to a line. The details about how it works may be found by going to the Help section in the LabVIEW program. The error associated with the fitting is calculated using inference for regression. This was suggested by ??? in the Statistics department at BYU as the correct way to calculate the error due to fitting data to a line. The standard error is given by

$$SE = s\sqrt{\frac{1}{n} + \frac{(x^* - \bar{x})^2}{\sum(x - \bar{x})^2}} \tag{3.4}$$

Where n is the number of source intensity measurements, x^* is position that is being evaluated, and s is given by

$$s = \sqrt{\frac{1}{n-2}\sum(y - \hat{y})^2} \tag{3.5}$$

Where $\hat{y}$ is the calculated source intensity.

The total error of the source intensity is combined with the "shot noise" error of the reflected intensity by summing the squares of the fractional standard deviations. This assumes the "shot noise" and fitting error are uncorrelated. This is a valid assumption because the source intensities and reflected intensities are measured at separate times. This would not be true if a two detector setup was used because the source intensity variations would be measured at the same time the reflected intensity was measured. The fractional standard deviation is

$$S = \frac{s}{X} \tag{3.6}$$

The combined standard deviation is then given by

$$S_{tot} = \sqrt{S_1^2 + S_2^2} \tag{3.7}$$

3.3.2 Test for Goodness of Fit

This section follows the discussion in reference [30]. The χ^2 test is used to test if the error bars calculated using the standard deviation are reliable. The χ^2 test assumes the distribution is Gaussian and compares the relative difference between the fit reflectance and the measured reflectance to the standard deviation.

$$\chi^2 = \sum_{k=1}^{n} \frac{(O_k - E_k)^2}{E_k} \tag{3.8}$$

where n is the total number of measurements. The fit is considered good if $\chi^2 < n$ and poor if $\chi^2 \gg n$.

Degrees of Freedom and Reduced χ^2

A better way of testing the goodness of a fit is to compare χ^2 to the degrees of freedom instead of n the number of data points. Depending on the data or the complexity of the fit there will fewer degrees of freedom compared to the number of data points. Another way to look at it to say each data point carries information. For each parameter fit to the data is uses that information, and it cannot be used to calculate other parameters including χ^2. The number of degrees of freedom is easily calculated

$$d = n - c \tag{3.9}$$

where n is the number of data points and c is the number of constraints or parameters that are being fit to the data set. Using this definition the expected value of χ^2 should be d the degrees of freedom.

$$\chi^2_{expected} = d \tag{3.10}$$

This may be taken a set further by dividing χ^2 by d to get the reduced chi squared or the chi squared per degree freedom.

$$\tilde{\chi^2} = \chi^2/d \tag{3.11}$$

Now the expected value of $\tilde{\chi^2}$ should be 1 or smaller. This is only approximate, if $\tilde{\chi^2} \sim 1$ the fit

may still be good. But if $\tilde{\chi^2} \gg 1$ then there is significant error in the fit. The reduced chi^2 of the fit n,k values is much greater than one. The fits appear to follow the data, but the error bars associated with the data only describe the statistical error in the data. There is still systematic error that is present in the data. The large value of the reduced χ^2 is indicative of systematic error in the data. The systematic error may be estimated to obtain a smaller reduced chi^2 but this was not done because of time constraints.

Chapter 4

Atomic Scattering Theory

The second purpose of this thesis is to determine what is the error associated with using atomic scattering factors (ASF) to determine the optical constants in the EUV. This can be done by seeing where the atomic scattering factors of graphite and diamond are significantly different. The definition of significantly different will depend on the application.

To compare data to a theory requires at least a working understand of the theories to be tested. Atomic scattering theory is very good at predicting the optical properties of a material in certain regimes of the electromagnetic spectrum. All theories make assumptions to make the it possible to find an analytic solution. Only a first principles calculation that makes no assumptions will accurately predict the optical properties of a material.

Only atomic scattering factors will be covered in the body of this thesis but Drude theory and Lorentz osciltor theory are covered in Appendix 4.20.

4.1 Independent Atom Approximation

At high enough energies (typically > 50 eV) it is possible to assume that only the core electrons participate in the determination of the optical properties of a material. If the light has enough energy it will interact with a fixed number of core electrons. If the light is higher or lower in energy different groups of core electrons will be involved in the interaction with the light. Eventually at high enough energies all the electrons in the atom will be involved in the interaction.

It would be nice to determine how many electrons are participating in the interaction with the incoming light. It would be even better if at high energies the parameter the represents the index of refraction would equal the atomic number of the element. I.E., carbon has six electrons so at high energies this parameter would be six. This means that all the electrons in a carbon atom are interacting with the light by reflecting or refracting the light. Besides using Krames-Kronig relations to check the validity of the calculated optical constants it would be a simple check to make sure the high energy representation was six.

This theory is know as atomic scattering factors (ASF). It is based on classical physics that describes each electron as a point charge that scatters light in many directions. Say at some energy four electrons are interacting with the light. Multiply the scattering effects of a classical electron scattering light by four to get effective scattering of the atom. This is not a perfect example but it illustrates the point. Imagine stirring gold flakes into a bucket of water and measuring the reflectance of the water and how much light it transmitted through the water. If more gold flakes are added to the water more light will be reflected and less light will pass through the water. This is similar to having a lot electrons that scatter light strongly participate in the interaction with the light.

What if instead of gold the flakes were bits of glass. Even though there are many pieces of glass that can scatter the light not much is scattered because the glass is transparent to the light. This is very similar to high energy light interacting with some material with a lot of electrons. Even though there are a lot of electrons that are influenced by the light the electrons themselves do not scatter the light very much so for the most part the light passes through with little refraction, reflection, or absorption.

The following discussion closely follows the discussion in reference [17].

4.1.1 Scattering Cross Sections

Before launching into the discussing of ASF it is important to review scattering cross sections. The ASF theory is based on comparing the scattering cross section of an atom to the scattering cross section of a single electron. From a conceptual point of view the scatting cross section describes how "wide" an object looks to something else that could hit it. A barn will have a larger scattering cross section than fly because it is easier to hit. Unlike a balls bouncing off the side of a barn light scattering off an electron or atom scattering into all directions.

From an E&M description the scattering cross section is defined as the scattered power divided by the intensity of the incident beam.

$$\sigma \equiv \frac{\bar{P}_{scatt}}{|\bar{\mathbf{S}}_\mathbf{i}|} \tag{4.1}$$

Where the bar means quantity is the time average. Power has units of watts, intensity has units of watts/m^2, so P/S has units of area. So now there is a way to relate the light scattered by an electron or atom to the apparent area of the electron.

4.1.2 Scattering of a Single Free Electron

Start by looking at the scattering of a single free electron. Why free? The electrons are bound to the atom. At high energies the electron that is bound to the atom by energies that are much smaller that the energy of the light. So the electron behaves as though it were free to the incident light. This assumption breaks down around band edges where the binding energy of the electron is comparable to the energy of the incoming light. It also breaks down for low energy light. How strong is the fall off? That is what this thesis HOPES to SHOW.

As with most classical phenomena involving charges and electrons start with the Lorentz force law

$$\mathbf{f} = m\mathbf{a} = -e(\mathbf{E} + \mathbf{v} \times \mathbf{B}) \tag{4.2}$$

This can be simplified by assuming the electron does not approach relativistic speeds and remembering $\mathbf{B} = \mathbf{E}/c$. The acceleration on the electron due to the magnetic field is several orders of magnitude smaller that the acceleration due to the electric field.

The acceleration of the electron has the form

$$\mathbf{a} = -\frac{e}{m}\mathbf{E} \tag{4.3}$$

The amplitude of the scattered electric field depends on the transverse acceleration of the electron.

$$a_T = a\sin\theta = -\frac{e}{m}\mathbf{E} \tag{4.4}$$

The scattered electric field depends on the acceleration of the charge.

$$E = -\frac{e^2 E\sin\theta}{4\pi\epsilon_0 mc^2 r}e^{-i\omega(t-r/c)} \tag{4.5}$$

All of the constants can be defined to be the classical electron radius.

$$r_e = \frac{e^2}{4\pi\epsilon_0 mc^2} \tag{4.6}$$

Now relate $\bar{P}_{scatt}$ to the scattered electric field and $|\bar{S}_i|$ to the incident electric field. From any senior level E&M book the dipole radiation from an accelerated electron is

$$P = \frac{8\pi}{3}\left(\frac{e^2|\mathbf{a}|^2}{16\pi^2\epsilon_0 c^3}\right) \tag{4.7}$$

The incident intensity may be calculated using the Poynting vector

$$\bar{\mathbf{S}} = \frac{1}{2}(\mathbf{E} \times \mathbf{H}^*) \tag{4.8}$$

Then using $\mathbf{E} = \mathbf{B}/c$ equation 4.8 becomes

$$\sqrt{\frac{\epsilon_0}{\mu_0}}|\mathbf{E}|^2 \tag{4.9}$$

Now put it all together using the acceleration given by equation 4.4.

$$\sigma = \frac{\bar{P}_{scatt}}{|\bar{\mathbf{S}}_\mathbf{i}|} = \frac{\pi}{3}\frac{e^4\sqrt{\mu_0}}{2m^2pi^2\sqrt{\epsilon_0}c^3} \tag{4.10}$$

With a little work using $c = (\epsilon_0\mu_0)^{-1/2}$ the last part of equation 4.10 can be made to look like r_e. The scattering cross section of an electron is given by

$$\sigma_e = \frac{8\pi}{3}r_e^2 \tag{4.11}$$

This result was first obtained by J.J. Thompson [].

4.1.3 Scattering by a Multi-Electron Atom

To model the scattering by a multi-electron one of two approaches may be taken. It may be assumed the wavelength of the light is large compared to the atomic distances. This assumption was used in section **??** to say the electric field over a region is a constant so the calculation is easier. It effectively smears out the electronic distribution of the atom. But ASF are most commonly used at short wavelengths where this assumption does not hold. It is important to define the electron distribution within the atom. One way it may be expressed, assuming the electrons are distinct points represented by delta functions.

$$\frac{N(\mathbf{r},t)}{R} = n(\mathbf{r},t) = \sum_{s=1}^{Z}\delta[\mathbf{r} - \Delta\mathbf{r}_s(t)] \tag{4.12}$$

The current density is found by multiplying the electron distribution by the velocity of the each of the electrons.

$$\mathbf{J}(\mathbf{r},t) = \sum_{s=1}^{Z}\delta[\mathbf{r} - \Delta\mathbf{r}_s(t)]\mathbf{v}_s(t) \tag{4.13}$$

It is assumed the $\mathbf{v}_s(t)$ term is driven by the incoming field and is not affected by fields scattered off of neighboring electrons. This assumption is known as the Born approximation.

If you are reading and haven't had a great deal of experience with E&M or Fourier transforms this next part will seem very opaque. If you don't have much E&M experience and you have made it this far, Congratulations. The next several step depend heavily on Fourier transforms. For some problems it is easier to transform a problem from position space to momentum or wave number space. On the surface it may seem to complicate the problem, but it actually makes it possible to solve the problem. Two transforms will be used to take $\mathbf{r} \rightarrow \mathbf{k}$ and $t \rightarrow \omega$. Use $\mathbf{J}(\mathbf{k},t)$ to solve for $\mathbf{E}(\mathbf{k},\omega)$. Then take the inverse Fourier transform to get $\mathbf{E}(\mathbf{r},t)$.

First Fourier transform (FT) $\mathbf{J}(\mathbf{r},t)$

$$\mathbf{J}_{k\omega} = \int_{\mathbf{r}}\int_{t}\mathbf{J}(\mathbf{r},t)e^{i(\omega t-\mathbf{k}\cdot\mathbf{k})}d\mathbf{r}\,dt \tag{4.14}$$

Now use the representation of the current density from equation 4.13 in the above equation

$$\mathbf{J}_{k\omega} = -e\sum_{s=1}^{Z}\int_{\mathbf{r}}\int_{t}\delta[\mathbf{r}-\Delta\mathbf{r}_s(t)]\mathbf{v}_s(t)e^{i(\omega t-\mathbf{k}\cdot\mathbf{k})}d\mathbf{r}\,dt \tag{4.15}$$

The delta function of $\mathbf{r}$ one of the integrations easy by collapsing the $\mathbf{r}$ integral. This does assume the time dependence of the $\Delta\mathbf{r}_s$ term is negligible compared to other time constraints in the integral. This also means the electrons move slowly in the atom compared to the oscillation of the field in the atom. Given these assumptions the current density now looks like

$$\mathbf{J}_{k\omega} = -e\sum_{s=1}^{Z}e^{-i\mathbf{k}\cdot\mathbf{k}}\int_{t}\mathbf{v}_s(t)e^{i\omega t}dt \tag{4.16}$$

The remaining integral is still a FT. It takes the velocity from time space into frequency space.

$$\mathbf{J}_{k\omega} = -e\sum_{s=1}^{Z}e^{-i\mathbf{k}\cdot\mathbf{k}}\mathbf{v}_s(\omega) \tag{4.17}$$

Now put this result into the electric field the is FT into $\mathbf{k}$ and ω space [17].

$$\mathbf{E}(\mathbf{r},t) = \frac{-i}{\epsilon_0(2\pi)^4}\int_{\mathbf{k}}\int_{\omega}\omega\frac{\mathbf{J}_{T_{k\omega}}e^{-i(\omega t-\mathbf{k}\cdot\mathbf{r})}d\mathbf{k}\,dr}{\omega^2-k^2c^2} \tag{4.18}$$

where $\mathbf{J}_{T_{k\omega}}$ is the transverse current density in the atom of interest. Only the electrons that are moving in the transverse direction to the observation point will produce fields that will be detected. Now explicitly write out the components in the current density and factor the denominator knowing the solution will require contour integration.

$$\mathbf{E}(\mathbf{r},t) = \frac{ie}{\epsilon_0(2\pi)^4}\sum_{s=1}^{Z}\int_{\mathbf{k}}\int_{\omega}\omega\frac{e^{-i\mathbf{k}\cdot\boldsymbol{\Delta}\mathbf{r}}\mathbf{v}_s(\omega)e^{-i(\omega t-\mathbf{k}\cdot\mathbf{r})}d\mathbf{k}\,dr}{(\omega-kc)(\omega+kc)} \tag{4.19}$$

The radial parts in the exponents may be combined into a single expression by looking at the relative geometry of $\mathbf{r}$ and $\Delta\mathbf{r}_s$. PUT IN A FIGURE THAT SHOWS THE GRAPHICAL REPRESENTATION OF Rs

$$\mathbf{r}_s \equiv \mathbf{r}-\Delta\mathbf{r}_s \tag{4.20}$$

Using the above definition and combining the terms in the exponents equation 4.19 may be written as where $\mathbf{r}_s$ points from the source to the observation point.

$$\mathbf{E}(\mathbf{r},t) = \frac{ie}{\epsilon_0(2\pi)^4}\sum_{s=1}^{Z}\int_{\mathbf{k}}\int_{\omega}\omega\frac{e^{-i(\mathbf{k}\cdot\mathbf{r}_s-\omega t)}\mathbf{v}_s(\omega)d\mathbf{k}\,dr}{(\omega-kc)(\omega+kc)} \tag{4.21}$$

This integration may be evaluated using contour integration. There are two simple poles of order 1 at $k = \pm\omega/c$. To complete the integral it must be assumed that k has an imaginary component. This makes the $e^{i\mathbf{k}\cdot\mathbf{r}}$ term in the numerator go to zero when $\mathbf{k}$ is large and imaginary during the contour integration. The contour is closed in the upper half plane to make the numerator go to zero[1]. The imaginary component of $\mathbf{k}$ also brings the poles off the real axis so the pole is completely enclosed in the contour. The pole being entirely enclosed is only makes the algebra slightly easier and is not crutial, assuming the integral did not blow up for large values of $\mathbf{k}$. There a several more details that are needed to finish the problem that may be found in reference [17]. The after the contour integration equation 4.21 looks like

$$\mathbf{E}(\mathbf{r},t) = \frac{e}{\epsilon_0(2\pi)^4}\sum_{s=1}^{Z}\frac{1}{r_s}\int_{-\infty}^{\infty}(-i\omega)\mathbf{v}_s(\omega)e^{-i\omega(t-r/c)}\,d\omega \tag{4.22}$$

All that is left is to evaluate the ω integral. First recognize that the $-i\omega$ comes from taking the derivative of the exponent. Because $\mathbf{v}_s(\omega)$ does not depend on t equation 4.22 may be written as

$$\mathbf{E}(\mathbf{r},t) = \frac{e}{\epsilon_0(2\pi)^4}\sum_{s=1}^{Z}\frac{1}{r_s}\int_{-\infty}^{\infty}\frac{d}{dt}(\mathbf{v}_s(\omega)e^{-i\omega(t-r/c)})\,d\omega \tag{4.23}$$

This is verified by taking the derivative. Now let $t' = t - r/c$ and pull the derivative out of the integral[2]. Equation 4.23 now becomes

$$\mathbf{E}(\mathbf{r},t) = \frac{e}{\epsilon_0(2\pi)^4}\sum_{s=1}^{Z}\frac{1}{r_s}\frac{d}{dt}\int_{-\infty}^{\infty}(\mathbf{v}_s(\omega)e^{-i\omega(t')})\,d\omega \tag{4.24}$$

Which is the inverse Fourier transform back to a retarded time domain. The extra r/c comes from the extra time it takes the fields to reach the observation point. The electric field a function of space and time is now

$$\mathbf{E}(\mathbf{r},t) = \frac{e}{(4\pi)\epsilon_0 c^2}\sum_{s=1}^{Z}\frac{1}{r_s}\frac{d}{dt}\mathbf{v}_s(\omega(t-r/c)) \tag{4.25}$$

Evaluate the time derivative to get the acceleration and use the expression for retarded time instead of t'.

$$\mathbf{E}(\mathbf{r},t) = \frac{e}{\epsilon_0(2\pi)^4}\sum_{s=1}^{Z}\frac{\mathbf{a}_{T,s}(\omega(t'))}{r_s} \tag{4.26}$$

The term inside the sum is the electric field radiated by an accelerated electron [18]. The sum allows the influence of more than one electron to taken account of.

Several things can now be said about the analysis so far. First start by exactly defining the positions of the electrons inside the atom. Then define $\mathbf{J}$, FT $\mathbf{J}$ and use it to calculate the FT of the electric field. Solve the inverse FT to get $\mathbf{E}$ as a function of $\mathbf{r}$ and t, and what comes out? An expression for the electric field that could have been obtained by summing the field coming from individual electrons accounting for the distance and retarded time of each electron. What this really means is that each

[1] If there was an extra negative sign in the exponent the contour could be closed in the lower half plane with the same result.

[2] Switching the order of integration and differentiation of two variables is not always this easy, but it can be done in a general way.

electron is behaving as though it was in a vacuum. This is sometimes called the Independent Atom Approximation. This should be what was expected because the interaction between neighboring electrons was assumed to be small and was ignored. So the definition of **J** is what really makes the electrons behave like isolated charged particles. This is very similar to section **??** where the electrons are assumed to be driven by the incident electric field and the interactions between the electrons is negligable. These approximations still allow for a good result because of the positive nuclei that help screen out the repulsive Coulombic forces. For high energies this is a good approximation for ASF because each electron is essentially free compared to the binding energies of the electrons. For the EUV this is not true. The energies of the electrons and their electrons becomes more important than it is for ASF in the x-ray portion of the spectrum.

Equations of Motion

Now write out the equation of motion. Assume there is a damping term that is proportional to γ and a restoring force that is proportional to ω_s^2. The electric field provides the driving force. As always, any contribution to the force from the magnetic field is ignored.

$$m\frac{d^2\mathbf{x}_s}{dt^2} + m\gamma\frac{d\mathbf{x}_s}{dt} + m\omega_s^2\mathbf{x}_s = -e\mathbf{E}_i \tag{4.27}$$

This equation can be solved by assuming the motion is oscillitory and at the same frequency as the incoming wave.

$$\mathbf{x}_s(t) = \mathbf{x}_s e^{-i\omega t} \tag{4.28}$$

Putting this into equation 4.27 and taking the deriviatives.

$$m(-i\omega)^2\mathbf{x}_s(t) + m\gamma(-i\omega)\mathbf{x}_s(t) + m\omega_s^2\mathbf{x}_s(t) = -e\mathbf{E}_i \tag{4.29}$$

Explicitly write out the spatial and time dependent parts of $\mathbf{E}_i$.

$$\mathbf{E}_i(\mathbf{r},t) = \mathbf{E}_i e^{-i(\omega t - \mathbf{k}_i\cdot\Delta\mathbf{r}_s)} \tag{4.30}$$

Combine equations 4.29 and 4.30, and solve for $\mathbf{x}_s(t)$.

$$\mathbf{x}_s(t) = \frac{1}{\omega^2 - \omega_s^2 + i\gamma\omega}\frac{e}{m}\mathbf{E}_i e^{-i(\omega t - \mathbf{k}_i\cdot\Delta\mathbf{r}_s)} \tag{4.31}$$

Take two time derivative to get the acceleration.

$$\mathbf{x}_s(t) = \frac{-\omega^2}{\omega^2 - \omega_s^2 + i\gamma\omega}\frac{e}{m}\mathbf{E}_i e^{-i(\omega t - \mathbf{k}_i\cdot\Delta\mathbf{r}_s)} \tag{4.32}$$

Multiply this result by $\sin\Theta$ to get $\mathbf{a}_{T,s}$. Then substitute into equation 4.26

$$\mathbf{E}(\mathbf{r},t) = \frac{e^2}{4\pi\epsilon_0 mc^2}\sum_{s=1}^{Z}\frac{\omega_s^2 E_i\sin\Theta}{\omega^2 - \omega_s^2 + i\gamma\omega}\frac{1}{r_s}e^{-u[\omega(t-r_s/c) - \mathbf{k}_i\cdot\Delta\mathbf{r}_s]} \tag{4.33}$$

The front term may be recognized as the classical electron radius (see 4.6). From figure **??** it can

be seen that if $r \gg \Delta r_s$ then the angle between r and r_s will be very small. Any correction may be approximated as subtracting the projection of $\Delta\mathbf{r}_s$ from r. This should almost always be a good correction because most experimental measurements are much larger than the beam spot on the sample.

$$r_s \simeq r - \mathbf{k}_0 \cdot \Delta\mathbf{r}_s \tag{4.34}$$

Now gather like terms, and make the further simplification that the correction to r_s is most important in the calculating the relative phase. The amplitude term can be simplified as r assuming the slight change in distance will not significantly change the amplitude.

$$\mathbf{E}(\mathbf{r},t) = \frac{e^2}{4\pi\epsilon_0 mc^2}\sum_{s=1}^{Z}\frac{\omega_s^2 E_i \sin\Theta}{\omega^2-\omega_s^2+i\gamma\omega}\frac{1}{r}e^{-u[\omega(t-r/c)+\omega(\frac{\mathbf{k}_0\cdot\Delta\mathbf{r}_s}{c})-\mathbf{k}_i\cdot\Delta\mathbf{r}_s]} \tag{4.35}$$

Write $k\mathbf{k}_0 = \mathbf{k}$ and remember that $\omega/c = k$ to simplify the phase term that depends on $\mathbf{k}$.

$$\mathbf{E}(\mathbf{r},t) = \frac{e^2}{4\pi\epsilon_0 mc^2}\sum_{s=1}^{Z}\frac{\omega_s^2 E_i \sin\Theta}{\omega^2-\omega_s^2+i\gamma\omega}\frac{1}{r}e^{-i[\omega(t-r/c)+(\mathbf{k}-\mathbf{k})\cdot\Delta\mathbf{r}_s} \tag{4.36}$$

The phase term may be simplified further by defining

$$\Delta\mathbf{k} = \mathbf{k} - \mathbf{k}_i \tag{4.37}$$

Where $\Delta\mathbf{k}$ is related to the material scattering the light into specific directions that depend on the structure of the material. From figure **??** it is possible to write Bragg's law of diffraction

$$|\Delta\mathbf{k}| = 2k_i \sin\theta \tag{4.38}$$

How does Bragg's law of diffraction come out of trying to calculate optical properties of materials? By defining $\Delta\mathbf{k}$ it was implicitly stating that this material will not scatter light into all direction, but into specific directions depending on how the electrons are bunched together. It is also stating that the electron bunches are not uniformly distributed though the material, but that they may be found in periodic bunches centered around specific points (i.e. nuclei) in the solid.

One last time write out all the details of the electric field

$$\mathbf{E}(\mathbf{r},t) = -\frac{r_e}{r}\left[\sum_{s=1}^{Z}\frac{\omega_s^2 e^{-\Delta\mathbf{k}\cdot\Delta\mathbf{r}_s}}{\omega^2-\omega_s^2+i\gamma\omega}\right]E_i\sin\Theta e^{-i\omega(t-r/c)} \tag{4.39}$$

Where the term in square brackets is the complex atomic scattering factor.

$$f(\Delta\mathbf{k},\omega) = \sum_{s=1}^{Z}\frac{\omega_s^2 e^{-\Delta\mathbf{k}\cdot\Delta\mathbf{r}_s}}{\omega^2-\omega_s^2+i\gamma\omega} \tag{4.40}$$

Write the electric field in terms of the ASF.

$$E(\mathbf{r},t) = -\frac{r_e f(\Delta\mathbf{k},\omega)E_i\sin\Theta}{r}e^{-i\omega(t-r/c)} \tag{4.41}$$

The scattering cross section of a single free electron E_{e^-} is given section 4.1.2.

$$E_{e^-} = -\frac{r_e E_i \sin\Theta}{r} e^{-i\omega(t-r/c)} \tag{4.42}$$

By combining equations 4.41 and 4.42 the field scattered by a multi-electron can be written as

$$E(\mathbf{r},t) = f(\Delta\mathbf{k},\omega)E_{e^-} \tag{4.43}$$

It is easy to see the ASF is a unitless parameter that relates the scattering of a multi-electron atom to the fields scattered by a single free electron.

The scattering cross section of a multi-electron atom is

$$\frac{8\pi}{3}|f|^2\mathbf{r}_e^2 \tag{4.44}$$

where f is the complex ASF.

The ASF as currently written is still difficult to use because the $\Delta\mathbf{k}\cdot\Delta\mathbf{r}_s$ does not simplify and can take on many values depending on the particular details of the situation.

Use the equation 4.38 with $k_i = 2\pi/\lambda$ to get

$$\Delta k = \frac{4\pi a_0}{\lambda}\sin\theta \tag{4.45}$$

Now take the dot product of $\Delta\mathbf{k}$ and $\Delta\mathbf{r}$ and assume the magnitude of δr is about the size of an atom. For convenience use the Bohr radius a_0.

$$|\Delta\mathbf{k}\cdot\Delta\mathbf{r}| \leq \frac{4\pi a_0}{\lambda}\sin\theta \tag{4.46}$$

The phase dependence will be negligible in two cases

$$a_0/\lambda \ll 1 \tag{4.47}$$

$$\theta \ll 1 \tag{4.48}$$

If either one or both of these two situations are satisfied the phase dependence drops out of the the equation so the ASF may be expressed as

$$f^0 = \sum_{s=1}^{Z} \frac{\omega^2}{\omega^2 - \omega_s^2 + i\gamma\omega} \tag{4.49}$$

Where the superscript zero represents this is only valid for situations where the phase dependence is neglible.

Other Regions where f^0 is not valid

The simplified expression of f^0 is a good approximation when the two previous conditions are met. This approximation is not valid around atomic resonance because the mechanics of the transitions are not adequately described by the semi-classical model that was used to derive f^0. Even though

equation 4.47 may hold for visible light ASF do not adequately describe the optical properties of a material because the energy of the light is too low to access electrons that provide most of the interactions that are assumed in the derivation of the atomic scattering factors.

Relate ASF to n,k

Is section **??** the optical constants n and k were derived by assuming there were oscillators in the material that interacted with the light at different frequencies. By comparing equation SOMETHING and SOMETHING ELSE there a simple relationship that relates the complex index of refraction to the atomic scattering factors.

$$n(\omega) = 1 - \delta + i\beta = 1 - \frac{n_a r_e \lambda^2}{2\pi}(f_1^0 - i f_2^0)ya \tag{4.50}$$

4.2 Sum Rules and Kramers-Kronig Relations

The theory of sum rules and Kramers-Kronig relations is different from the previous three theories of this chapter. Drude theory, Lorentz oscillators, and ASF are used to better understand or predict the optical properties of materials at various wavelengths of light. Sum rules relations are used to check the validity of optical constant by "counting" the number of electrons that are involved in interactions with light. Kramers-Kronig relations are used to calculate the imaginary part of the index of refraction using the real part of the index of refraction or visa versa. Both of these methods are extremely useful in verifying the validity of an optical constant data set.

4.2.1 Sum Rules

The discussion of sum rules follows directly from the discussion of atomic scattering factors (see section 4.1 and closely follows the discussion in [17]. The last equation in section 4.1 showed the ASF being a sum of oscillators.

$$f^0 = \sum_{s=1}^{Z} \frac{\omega^2}{\omega^2 - \omega_s^2 + i\gamma\omega} \tag{4.51}$$

At low energies the sum will only include those electrons that are influenced by the light and will not include the influence of the core electrons because the light does not have sufficient energy. Equation 4.49 may be written as

$$f^0 = \sum_{s=1}^{N(\omega)} \frac{\omega^2}{\omega^2 - \omega_s^2 + i\gamma\omega} \tag{4.52}$$

Where $N(\omega)$ denotes the number of electrons that will be involved in the scattering depends on the frequency of the light used to probe the material.

Closely related to the oscillators at each ω_s is an oscillator strength g_s that corresponds to the values of ω_s. In the semi-classical model that is being used in this thesis g_s is an integer value that represents the number of electrons that are involved in a given resonance frequency.

$$f^0 = \sum_{s} g_s = Z \tag{4.53}$$

In carbon there are two K shell electrons, or two electrons that are more tightly bound to the nucleus than the other electrons. The ω_s associated with this resonance occurs at 284 eV (see figure 4.2.1.) Above this energy both electrons will be able to scatter light so the g_s associated with this is 2. It can also be seen in figure 4.2.1 that below this energy a carbon atom has four electrons ($N(\omega < \omega_K) = 6 - 2$) that participate in the scattering of light.

Integer values of g_s is an ideal case and can be made more general by allowing g_s to take on non-integer values. This corresponds to transition probabilities in quantum mechanics that themselves are not integer values (An atom is *slightly* more complicated that a collection of free electrons.) The sum rule still holds but the oscillator strengths are summed over the states in the atom

$$f^0 = \sum_{n} g_{kn} = Z \tag{4.54}$$

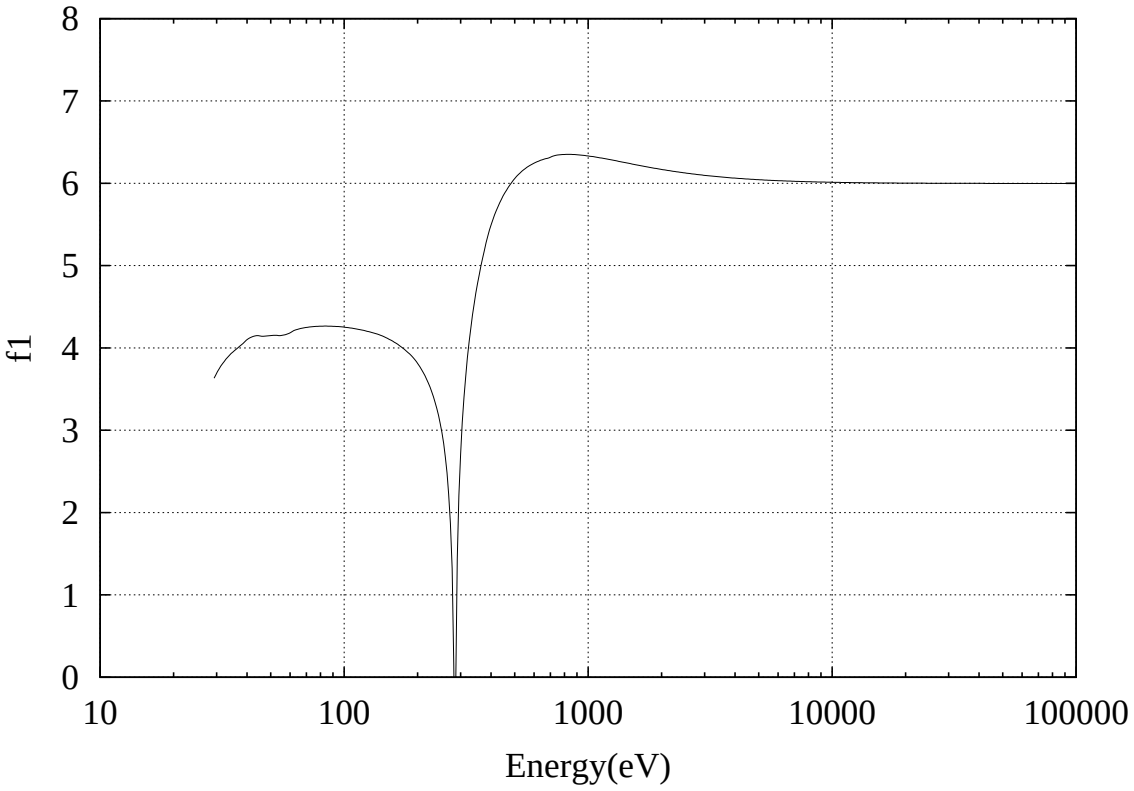

Figure 4.1: At high enough energies the value of f_1^0 of carbon (Z=6) goes to six. This shows that at high enough energies the atoms scatters light six times more than the light scattered by a single electron. That is what should be expected because there are six electrons in a carbon atom.

where k is the initial state and k is the final state. This is known as the Thomas-Reiche-Kuhn sum rule [19, 20, 21]. The ASF can now be written in terms of g_s

$$f^0 = \sum_s^Z \frac{g_s \omega^2}{\omega^2 - \omega_s^2 + i\gamma\omega} \tag{4.55}$$

For $\omega^2 \gg \omega_s^2$ equation 4.55 will simplify to

$$f^0(\omega) = \sum_s g_s \frac{\omega^2}{\omega^2} = \sum_s g_s \tag{4.56}$$

There are other forms of sum rules that may be used to verify the validity of a set of ASF. A explanation of the various sums rules can be found in reference [22].

4.2.2 Kramers-Kronig Relations

Kramers-Kronig relations are a mathematical argument involving functions that have coupled real and imaginary parts. The real and imaginary parts of optical constants are coupled because it is the same electrons that are involved in determining the optical properties of a solid. This is known as causality, or that the physical response described by optical constants is caused by the same physical mechanism. There are more subtle arguments that involve causality, but for the purposes of this thesis it is satisfactory to understand that if the way an electron scatters light can be described by n, then the same electron will also absorb light, described by k, in a way that is related to the way the electron scatters light. The two optical constants describe different material properties but they are fundamentally related. The analysis in this thesis will not involve Kramers-Kronig relations, but for completeness the forms of the integrals will be given. More details about evaluating Kramers-Kronig relations may be found in reference [22]. First assume the complex index of refraction is $\mathcal{N} = n + ik$.

$$\mathcal{R}\rceil[n^2(\omega_0) - 1] = \frac{2}{\pi} P \int_0^\infty \frac{\omega \mathcal{I}\Updownarrow[n^2(\omega) - 1]}{\omega^2 - \omega_0^2}\, d\omega \tag{4.57}$$

$$\mathcal{I}\Updownarrow[n^2(\omega_0) - 1] = -\frac{2}{\pi} P \int_0^\infty \frac{\omega_0 \mathcal{R}\rceil[n^2(\omega) - 1]}{\omega^2 - \omega_0^2}\, d\omega \tag{4.58}$$

Notice that to get a single value of n or k at a fixed ω_0 it is nescissary to know every value of the other optical constant at *every* ω. That is why it is important to know the optical constants for all frequencies.

Chapter 5

Data

The industrial diamond and graphite (HOPG) data reported in Chapter 4.20 will not be used in the analysis section of this thesis, because the data does not cover important features in the atomic scattering of carbon. Data from previously published data sets will be used for the analysis.

5.1 Summary of Optical Constants

First examine the atomic scattering factors of several references to determine which data set is the best to use for the analysis. To determine which data set to use plot the calculated atomic scattering factors of diamond, graphite, and amorphous carbon. Most of this data was found digitized and gathered in IMD [9].

Diamond and graphite have been measured previously and the optical properties are most often tabulated as n and k values or f1 and f2 values. The most common reference for n and k values is The Handbook of Optical Constants (HBOC) ed. E. Palik [2]. Optical constants are for cubic carbon (c-C, diamond) are tabulated in HBOC I or II and range between 600–10000Å. The optical constants for graphite (g-C) in HBOC I or II and range between 150–10000 Å.

Atomic scattering factors (f1 and f2) were first compiled in a comprehensive way by B.L. Henke et al [3]. The ASF tables have been updated since they were first published [4]. The data for the updates may be found in references [5, 6, 7, 8] and are cited in this thesis as taken from CXRO\LLNL [4]. ASF have also been calculated by Chantler using SOME METHOD.

Data from Henke [] and Chantler [] are reported as f1 and f2 data, but all other references [] report their data as n,k values. The n,k values are converted to f1 and f2 values by inverting equation 4.50. In general this conversion assumes the atomic scattering factors are independent of the density of the material. Here that assumption is ignored in the conversion because the f1 and f2 values will not be used for calculating the optical properties of a material for a real application.

$$f_1 + if_2 = \frac{\beta}{\lambda^2}(1 - n + ik) \tag{5.1}$$

$$\beta = \frac{2\pi W}{r_e \rho A}\left(1 \times 10^{-2} m\right)^3 \tag{5.2}$$

where W is the atomic weight in grams/mole, the cubed factor of $10^{-2}m$ is to convert cm to m, r_e is the classical electron radius, ρ is the density of the material in grams/cm^3, and A is Avogadro's number. This is the equation for a material made from one element. It is possible to calculate the optical constants of a compound by summing the indices of refraction weighted by their densities [17].

There are two preexisting references for the optical constants of diamond, but there is not good agreement between the two data sets. By comparing the optical constants of diamond to those of amorphous carbon and graphite it is possible to see the Palik data is more reliable. The optical constants of diamond measured by Windt were determined from a thin film sample of CVD diamond. The difference in the optical properties may be due to the difference between measuring a bulk film and thin film, but the surface of the diamond sample is reported in reference [10] to have visible surface irregularities.

After the data is collected using the VAR VI described in section 2.4 it is sent to another VI to calculate the reflectance and the error associated with each data point. After a reflectance curve has been calculated from the measured data it is entered into IMD to fit the optical constants of the material to the model described in section 3.2.2. IMD is also used to calculate the error associated with the fit optical constants by using the χ^2 test to calculate a confidence interval. Once that has been done the real data analysis can be started.

5.2 Data Analysis

The second purpose of this thesis is focused on determining the errors associated with using ASF to estimate the optical properties of materials in the EUV. That is done by calculating the relative difference between the optical constants of diamond and graphite (HOPG).

As previously mentioned in section 4.1 the atomic scattering factors give a measure of how may electrons are participating in some interaction with light. At high energies all the electrons are involved in the scattering of light, so it is expected that f1 will approach Z. But at low energies the number of electrons involved in the interaction with the light depends on the crystal properties of the light. ASF can still be calculated but they will be unique to the material that was measured and will not be easily transferable to another crystal phase of a similar material.

The difference may be shown by calculating the relative difference between the ASF of one crystal phase to another. The relative difference is calculated as may be expected

$$\Delta = \frac{f_{diamond} - f_{graphite}}{f_{graphite}} \tag{5.3}$$

The graphite data is used to normalize that data because as currently tabulated in HBOC II it has data tabulated farther into the EUV than diamond. Because graphite is an anisotropic material it has two sets of n,k values that depend on what direction the light is incident on the material. These two sets are averaged as explained in section **??** to get one set of ASF.

This shows the greatest difference can be seen in the difference between the f_1 values of the different materials. In the case of carbon the difference is pronounced above 750 Åor 16.5 eV.

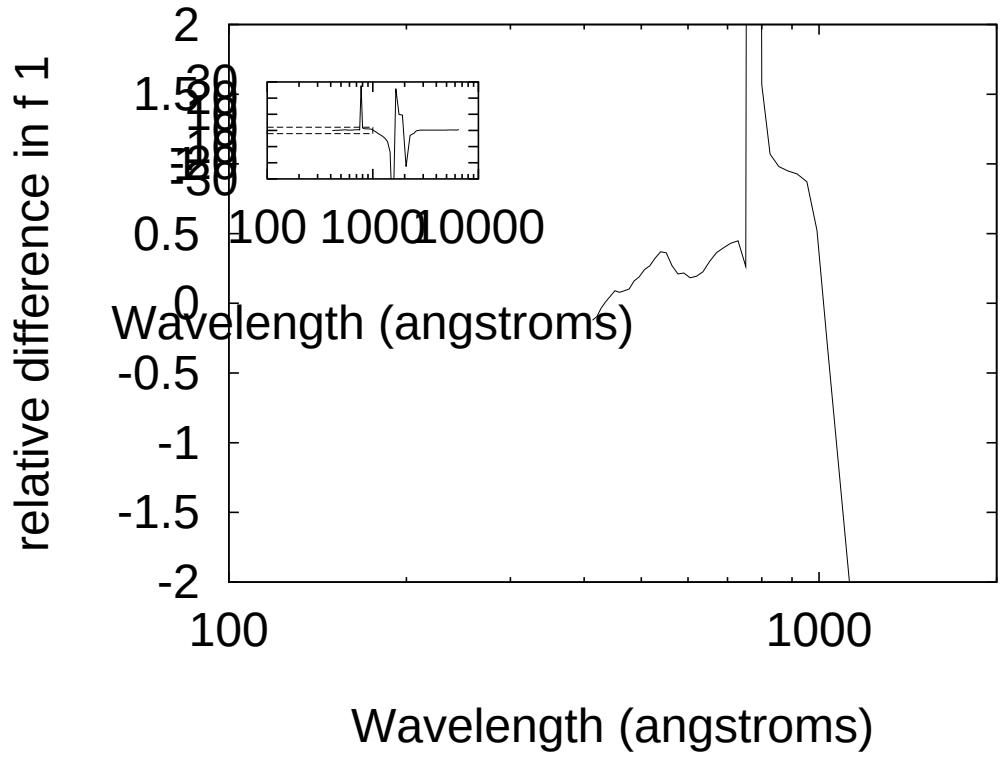

Figure 5.4: Atomic scattering data of g-C (graphite) calculated from optical constants in HBOC II. The ordinary, extraordinary, and "average" values for graphite are plotted. The atomic scattering factors of a-C (amorphous carbon) are included for a reference.

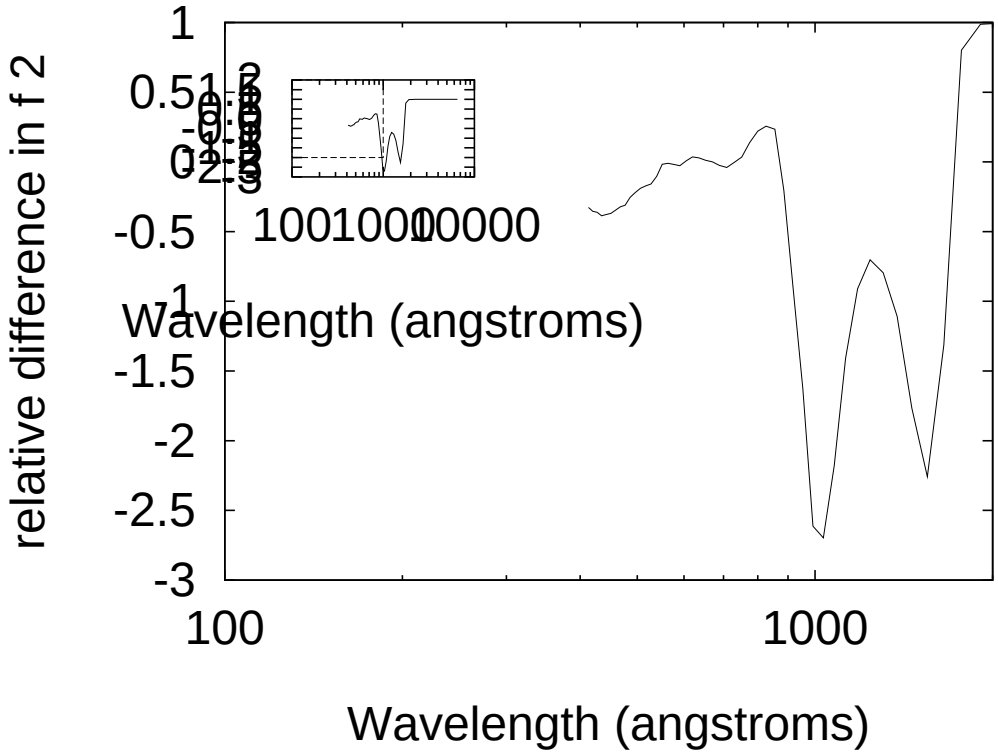

Figure 5.5: Atomic scattering data of g-C (graphite) calculated from optical constants in HBOC II. The ordinary, extraordinary, and "average" values for graphite are plotted. The atomic scattering factors of a-C (amorphous carbon) are included for a reference.

Chapter 6

Conclusions

A variable angle reflectometer was built to measure the absolute reflectance of surfaces over a wide range of angles. The usefulness of this chamber has been demonstrated by measuring the optical properties of industrial diamond and HOPG at multiple wavelengths in the EUV. The reflectance measuerments have been automated using LabVIEW to control the stepper motors and calculate the reflectance.

Atomic scattering factors are very useful for calculating the optical constants for soft and hard x rays. The assumptions used to simplify the calculations at high energies are not valid in the visible and IR portion of the spectrum. This is not a surprise because the theory is based on the assumption that the atoms are independent of the crystal phase of the material. By calculating the relative difference in the ASF of the material it is possible to quantify the error introduced by using ASF to calculate the optical constants of materials at wavelengths in the EUV.

The effect of this difference can be seen by looking at the reflectance of light normal to a surface in a vacuum given by

$$R = \frac{n-1}{n+1} \tag{6.1}$$

This assumes there is not absorption. Now assume that the index of refraction is actually $n + \Delta n$. Now equation 6.1 becomes

$$R = \frac{n+\Delta n-1}{n+\Delta n+1} \tag{6.2}$$

Expand the denominator using the binomial expansion to get back equation 6.1 plus the CORRECTION terms.

$$R = \frac{n-1}{n+1} + \frac{\Delta n}{n+1} + \frac{\Delta n(1-n-\Delta n)}{(n+1)^2} \tag{6.3}$$

If the correction term is some fraction of the original index of refraction, $\Delta n = cn$ it is possible to calculate the error in the reflectance as a function of the index and the fractional difference in the optical constants.

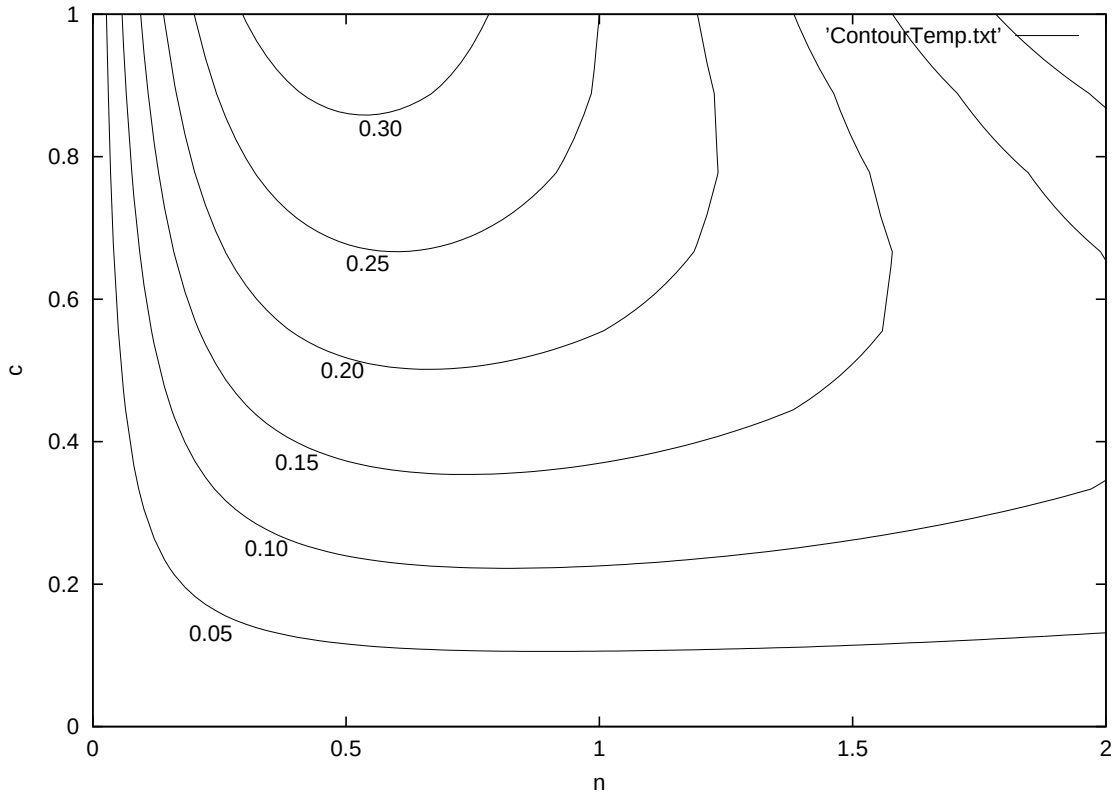

Figure 6.1: First order correction in reflectance as a function of the index of refraction and the fraction of change in the index of refraction.

Bibliography

[1] www.amptek.com. html document, 2001. Picture copied from web site.

[2] ed. Edward D. Palik. *Handbook of Optical Constants of Solids*. Academic Press, Orlando, 1985.

[3] E.M. Gullikson B.L. Henke and J.C. Davis. X-ray interactions: photoabsorption, scattering, transmission, and reflection at e=50-30000 ev, z=1-92. *Atomic Data and Nuclear Data Tables*, 54:181–342, 1993.

[4] Center for x-ray optics, materials sciences division, lbnl. html document, 2001. www-cxro.lbl.gov.

[5] R. Soufli and E. M. Gullikson. Absolute photoabsorption measurements of molybdenum in the range 60 to 930 ev for optical constant determination. *Applied Optics*, 1997.

[6] R. Soufli and E. M. Gullikson. Reflectance measurements on clean surfaces for the determination of optical constants of materials in the euv/soft x-ray region. *Applied Optics*, 1995.

[7] Y. S. Song H. L. Marshall M. L. Schattenburg D. E. Graessle K. A. Flanagan R. L. Blake J. Bauer E. M. Gullikson C. S. Nelson, T. H. Markert. Efficiency measurements and modeling of the advanced x-ray astrophysics facility (axaf) high-energy transmission gratings. *Proceedings of the SPIE*, 2280:191–203.

[8] S. Mrowka J. H. Underwood E. M. Gullikson, P. Denham. Absolute photoabsorption measurements of mg, al, and si in the soft-x-ray region below the l2,3 edges. *Physical Review B*, 49:16283–8.

[9] David L. Windt. Imd- software for modeling the optical properties of multilayer films. *Computers In Physics*, 1998.

[10] David L. Windt. *The Optical Properties of 21 Thim Film Materials in the 10 eV to 500 eV Photon Energy Range*. PhD thesis, University of Colorado, 1988.

[11] ed. Edward D. Palik. *Handbook of Optical Constants of Solids II*. Academic Press, Orlando, 1988 ?

[12] Jr. M. Scott P. Arendt B. Newnam ; R. F. Fisher A. B. Swartzlander P. Z. Takacs D. L. Windt, Webster C. Cash and J. M. Pinneo. Optical constants for thin films of c, diamond, al, si, and cvd sic ; from 24 to 1216 a. *App. Opt.*, 1988.

[13] D. W. Lynch J. H. Weaver, C. Krafka and E. E. Koch. *Physik Daten,Physics Data: Optical Properties of Metals*. Fach-information zentrum, 1981.

[14] N. D. Mermin Ascroft, N. W. *Solid State Physics*. Holt, Rinehart, and Winston, New York, 1976.

[15] Gerald Burns. *Solid State Physics*. Academic Press, Orlando, 1985.

[16] Rosenberg. *Solid State Physics*. Academic Press, Orlando, 1985.

[17] David T. Attwood. *Soft X-Rays and Extreme Ultraviolet Radiation*. Chambridge University Press, 2000.

[18] David J. Griffiths. *Introduction to Electrodynamics*. Prentice Hall, 1989.

[19] R.W James. *The Optical Principles of Diffraction of X-Rays*. Bell, 1962.

[20] R.L. Liboff. *Introductory Quantum Mechanics*. Addison-Wesley, 1998.

[21] J.C. Slater. *The Quantum Theory of Matter*. McGraw Hill, 1968.

[22] R. Soufli. *Optical Constants of Materials in the EUV/Soft X-Ray Region for Mulitlayer Mirror Applications*. PhD thesis, University of California at Berkeley, 1997.

[23] S. Kumar F. Paresce and C.S. Bowyer. Continuous discharge line source for the extreme ultraviolet. *Applied Optics*, 10:1904–1908.

[24] www.mcpherson-inc.com. html document, 2001. Picture copied from web site.

[25] Raymond A. Serway. *Physics, For Scientists and Engineers*. Saunders College Publishing, 1996.

[26] Wolf Born and Emil Wolf. *Principles of Optics*. Pergamon Press, 1959.

[27] Cynthia E. Mills. Multi-angle reflectance measurements in the euv. Honors Thesis, 2001.

[28] Shannon Lunt. The use of genetic algorithms in multilayer mirror optimization. Honors Thesis, 1999.

[29] N.C. Barford. *Experimental Meassurements: Precision, Error, and Truth*. John Wiley & Sons, 1985.

[30] John R. Taylor. *An Introduction to Error Analysis*. University Science Books, 1982.